The Koala: A Fast Blue Optical Transient with Luminous Radio Emission from a Starburst Dwarf Galaxy at $z = 0.27$

Anna Y. Q. Ho[1], Daniel A. Perley[2], S. R. Kulkarni[1], Dillon Z. J. Dong[1], Kishalay De[1], Poonam Chandra[3], Igor Andreoni[1], Eric C. Bellm[4], Kevin B. Burdge[1], Michael Coughlin[5], Richard Dekany[6], Michael Feeney[6], Dmitry D. Frederiks[7], Christoffer Fremling[1], V. Zach Golkhou[4,8,15], Matthew J. Graham[1], David Hale[6], George Helou[9], Assaf Horesh[10], Mansi M. Kasliwal[1], Russ R. Laher[9], Frank J. Masci[9], A. A. Miller[11,12], Michael Porter[6], Anna Ridnaia[7], Ben Rusholme[9], David L. Shupe[9], Maayane T. Soumagnac[13,14], and Dmitry S. Svinkin[7]

[1] Cahill Center for Astrophysics, California Institute of Technology, MC 249-17, 1200 E California Boulevard, Pasadena, CA 91125, USA; ah@astro.caltech.edu
[2] Astrophysics Research Institute, Liverpool John Moores University, IC2, Liverpool Science Park, 146 Brownlow Hill, Liverpool L3 5RF, UK
[3] National Centre for Radio Astrophysics, Tata Institute of Fundamental Research, PO Box 3, Pune, 411007, India
[4] DIRAC Institute, Department of Astronomy, University of Washington, 3910 15th Avenue NE, Seattle, WA 98195, USA
[5] School of Physics and Astronomy, University of Minnesota, Minneapolis, MN 55455, USA
[6] Caltech Optical Observatories, California Institute of Technology, Pasadena, CA 91125, USA
[7] Ioffe Institute, Politekhnicheskaya 26, St. Petersburg 194021, Russia
[8] The eScience Institute, University of Washington, Seattle, WA 98195, USA
[9] IPAC, California Institute of Technology, 1200 E. California Blvd, Pasadena, CA 91125, USA
[10] Racah Institute of Physics, The Hebrew University of Jerusalem, Jerusalem 91904, Israel
[11] Center for Interdisciplinary Exploration and Research in Astrophysics and Department of Physics and Astronomy, Northwestern University, 1800 Sherman Ave, Evanston, IL 60201, USA
[12] The Adler Planetarium, Chicago, IL 60605, USA
[13] Lawrence Berkeley National Laboratory, 1 Cyclotron Road, Berkeley, CA 94720, USA
[14] Department of Particle Physics and Astrophysics, Weizmann Institute of Science, Rehovot 76100, Israel

Abstract

We present ZTF18abvkwla (the "Koala"), a fast blue optical transient discovered in the Zwicky Transient Facility (ZTF) One-Day Cadence (1DC) Survey. ZTF18abvkwla has a number of features in common with the groundbreaking transient AT 2018cow: blue colors at peak ($g - r \approx -0.5$ mag), a short rise time from half-max of under two days, a decay time to half-max of only three days, a high optical luminosity ($M_{g,\text{peak}} \approx -20.6$ mag), a hot ($\gtrsim 40,000$ K) featureless spectrum at peak light, and a luminous radio counterpart. At late times ($\Delta t > 80$ days), the radio luminosity of ZTF18abvkwla ($\nu L_\nu \gtrsim 10^{40}$ erg s^{-1} at 10 GHz, observer-frame) is most similar to that of long-duration gamma-ray bursts (GRBs). The host galaxy is a dwarf starburst galaxy ($M \approx 5 \times 10^8\, M_\odot$, SFR $\approx 7\, M_\odot$ yr^{-1}) that is moderately metal-enriched ($\log[\text{O/H}] \approx 8.5$), similar to the hosts of GRBs and superluminous supernovae. As in AT2018cow, the radio and optical emission in ZTF18abvkwla likely arise from two separate components: the radio from fast-moving ejecta ($\Gamma\beta c > 0.38c$) and the optical from shock-interaction with confined dense material ($< 0.07\, M_\odot$ in $\sim 10^{15}$ cm). Compiling transients in the literature with $t_{\text{rise}} < 5$ days and $M_{\text{peak}} < -20$ mag, we find that a significant number are engine-powered, and suggest that the high peak optical luminosity is directly related to the presence of this engine. From 18 months of the 1DC survey, we find that transients in this rise-luminosity phase space are at least two to three orders of magnitude less common than CC SNe. Finally, we discuss strategies for identifying such events with future facilities like the Large Synoptic Survey Telescope, as well as prospects for detecting accompanying X-ray and radio emission.

Unified Astronomy Thesaurus concepts: Radio transient sources (2008); High energy astrophysics (739); Supernovae (1668); Core-collapse supernovae (304); Jets (870); Sky surveys (1464)

Supporting material: data behind figures

1. Introduction

Historically, the cadence of optical time-domain surveys was tuned to detecting SNe Ia, whose optical light curves rise from first light to peak in 15–20 days (Miller et al. 2020). Recognizing that this observing strategy resulted in "gaps" in timescale-luminosity phase space, surveys such as the Palomar Transient Factory (Law et al. 2009; Rau et al. 2009) and the Pan-STARRS1 Medium Deep Survey (Drout et al. 2014) sought to systematically chart the landscape of short-timescale (<10 day) phenomena. These efforts delineated populations of fast transients spanning many orders of magnitude in peak luminosity, from faint calcium-rich transients (Kasliwal et al. 2012) to luminous relativistic explosions (Cenko et al. 2013).

A population of particular recent interest is "fast-evolving luminous transients" (Rest et al. 2018) or "fast blue optical transients" (Margutti et al. 2019). A consistent definition of this "class" does not yet exist; these terms typically refer to transients with rise times and peak luminosities too fast and too luminous, respectively, to be explained by the radioactive decay of ^{56}Ni. Although they likely arise from a variety of progenitors, fast luminous transients are primarily found in star-forming galaxies (Drout et al. 2014; Pursiainen et al. 2018) and therefore are thought to represent a variety of poorly understood endpoints of massive-star evolution. As summarized in Kasen (2017), fast and luminous light curves may be

---

powered by shock breakout or shock-cooling emission from material that is closely confined to the progenitor star at the time of explosion, or alternatively by a "central engine:" accretion onto a black hole, or the rotational spindown of a magnetar.

Most fast luminous optical transients have been found in archival searches of optical-survey data, including PS1 (Drout et al. 2014), the Dark Energy Survey (Pursiainen et al. 2018), Kepler (Rest et al. 2018), and the Supernova Legacy Survey (Arcavi et al. 2016). A handful have been discovered while the transient was still active, enabling prompt follow-up observations. For example, spectroscopic monitoring of the fast luminous transients iPTF16asu (Whitesides et al. 2017; Wang et al. 2019) and ZTF18abukavn (SN 2018gep; Ho et al. 2019a) revealed that, as the optical emission faded, the spectrum developed features typical of broad-lined Ic SNe.

The discovery of the fast luminous transient AT2018cow (Prentice et al. 2018) generated considerable excitement because of its proximity ($z = 0.0141$) and the consequent opportunity for detailed observations. AT2018cow had several remarkable features: (1) near-relativistic ejecta velocities at early times, from optical spectroscopy (Perley et al. 2019a); (2) luminous and fast-varying X-ray emission suggesting an exposed central engine (Rivera Sandoval et al. 2018; Ho et al. 2019b; Margutti et al. 2019); (3) high-velocity emission lines of hydrogen and helium emerging at late times (Perley et al. 2019a); (4) no second peak that would indicate a significant role for radioactive ejecta in powering the light curve (Perley et al. 2019a); and (5) luminous submillimeter emission indicating a large explosion energy injected into a shell of very dense material (Ho et al. 2019b; Huang et al. 2019). Despite extensive observations across the electromagnetic spectrum, the progenitor of AT2018cow is unknown. One suggestion is a massive-star explosion that resulted in the formation of an accreting black hole or magnetar, which drove a mildly relativistic jet or wind (Ho et al. 2019b; Margutti et al. 2019; Perley et al. 2019a). Other suggestions include an electron-capture SN (Lyutikov & Toonen 2019) and a tidal disruption event (TDE; Vinkó et al. 2015; Kuin et al. 2019; Perley et al. 2019a). If AT2018cow was a massive-star explosion, the dense confined CSM points to eruptive mass loss shortly before core collapse (Ho et al. 2019b), and indeed, Fox & Smith (2019) pointed out the similarity between AT2018cow and interaction-powered Type Ibn SNe.

Here, we report the discovery in Zwicky Transient Facility (ZTF) data of ZTF18abvkwla,[16] a fast-rising luminous optical transient at $z = 0.27$.[17] In Section 2, we present the key observational features of ZTF18abvkwla—a rest-frame g-band light curve similar to that of AT2018cow, a luminous radio counterpart similar to gamma-ray burst (GRB) afterglows, and a starburst dwarf host galaxy. In Section 3, we compare ZTF18abvkwla to transients in the literature that have $t_{\rm rise} < 5$ days and $M < -20$ mag, where $t_{\rm rise}$ is defined from 0.75 mag below peak to peak (half-max to max in flux space). We use a cut of $M < -20$ mag to exclude "normal" Type Ibn SNe (Hosseinzadeh et al. 2017), and we exclude the hundreds of optical afterglows discovered in GRB follow-up observations (Kann et al. 2010). The comparison sample is shown in

Table 1 and Figure 1. Note that the Table 1 transients have thermal spectra at peak, unlike GRB afterglows (which arise from synchrotron radiation).

In Section 4.1, we model the optical emission from ZTF18abvkwla as thermal emission from shock breakout in dense confined material. In Section 4.2, we use the radio emission to estimate properties of the forward shock (velocity, shock energy) and the ambient medium. In Section 4.3, we discuss possible progenitor systems. Finally, in Section 5, we use 18 months of survey observations to estimate the rate of transients in the phase-space of Figure 1, and find that the rate is 2–3 times smaller than the CC SN rate.

Throughout this paper, we use a standard ΛCDM cosmology (Planck Collaboration et al. 2016) and times are reported in UT. Optical magnitudes are reported in the AB system (Oke & Gunn 1983), and corrected for foreground Galactic extinction using reddening measurements in Schlafly & Finkbeiner (2011) and the extinction law from Fitzpatrick (1999).

2. Discovery and Basic Analysis

2.1. Optical

2.1.1. Photometry

Since 2018 April, ZTF (Bellm et al. 2019b; Graham et al. 2019) has been conducting a wide-area (2000–3000 deg^2) one-day cadence (1DC) survey in g and r (Bellm et al. 2019a). The sky coverage of the 1DC survey is shown in Figure 2, and a histogram of the typical time between exposures is shown in Figure 3.

The IPAC ZTF pipeline (Masci et al. 2019) uses the method described in Zackay et al. (2016) to generate difference images using a coadded reference image. Every 5σ point-source detection is assigned a score based on a machine-learning real/bogus metric (Duev et al. 2019; Mahabal et al. 2019), and is cross-matched against external catalogs to search for resolved and extended counterparts (Tachibana & Miller 2018). Alerts are distributed in Avro format (Patterson et al. 2019) and are filtered by the ZTF collaboration using a web-based system called the GROWTH Marshal (Kasliwal et al. 2019).

ZTF18abvkwla was discovered in an image obtained on 2018 September 12. The alert passed a filter designed to look for rapidly evolving transients, and as a result we obtained a follow-up spectrum 24 hr later (Section 2.1.2). The discovery magnitude was $g = 19.73 \pm 0.16$ mag and the last nondetection was one day prior, with a limiting magnitude $g > 20.74$.

The source position was measured to be $\alpha = 02^{\rm h}00^{\rm m}15\overset{s}{.}19$, $\delta = +16^{\rm d}47^{\rm m}57\overset{s}{.}3$ (J2000), which is $0\overset{''}{.}28 \pm 0\overset{''}{.}13$ from the nucleus of a blue ($g - r = 0.32$ mag) extended source that has a photometric redshift of 0.11 (68 percentile confidence interval 0.08–0.29) in the eighth data release of LegacySurvey (DR8; Dey et al. 2019). At $z = 0.2714$ (Section 2.1.2), this offset corresponds to 1.9 ± 0.9 kpc. The host is approximately $2''$ (14 kpc) across.

The light curve (Figure 4; Table 2) has a similar timescale and peak luminosity to that of AT2018cow. In rest-frame g-band, the rise time is 1.83 ± 0.05 days, the fade time is 3.12 ± 0.22 days, and the peak magnitude is -20.59 ± 0.07 mag.

We estimate that the onset of the optical emission was around the time of the last nondetection ($t_0 = 2458372.9206$ JD), and we use this as a reference epoch for the remainder of the paper.

[16] Nicknamed "Koala" on account of the last four letters of its ZTF ID.
[17] After the submission of our paper, Coppejans et al. (2020) published radio and X-ray observations of CSS161010, another transient in a dwarf galaxy with properties similar to AT2018cow.

Table 1
Transients in the Literature with $t_{\rm rise} < 5$ days and $M < -20$ mag

Name	Redshift	$M_{g,\max}$	$t_{\rm rise}$ days	$t_{\rm fade}$ days	References
Dougie	0.19	-23.03 ± 0.13	3.92 ± 0.14	9.69 ± 1.19	(1)
SN 2011kl	0.677	-20.31 ± 0.13	4.97 ± 1.20	17.70 ± 5.82	(2), (3)
SNLS04D4ec	0.593	-20.26 ± 0.03	<3.81	8.60 ± 0.43	(4)
SNLS05D2bk	0.699	-20.39 ± 0.02	2.90 ± 0.06	12.75 ± 0.78	(4)
SNLS06D1hc	0.555	-20.28 ± 0.03	4.59 ± 0.06	12.35 ± 0.45	(4)
iPTF15ul	0.066	-21.2 ± 0.3	1.53 ± 0.05	3.72 ± 0.08	(5)
DES16X1eho	0.76	-20.39 ± 0.09	1.28–2.53	1.01 ± 0.27	(6)
iPTF16asu	0.187	-20.3 ± 0.1	1.14 ± 0.13	10.62 ± 0.55	(7)
AT2018cow	0.0141	-20.89 ± 0.06	1.43 ± 0.08	1.95 ± 0.06	(8), (9)

Notes. Timescales are presented in rest frame and measured using the light curve that most closely matches rest-frame g. Luminosity is corrected for Galactic extinction, assuming zero host-galaxy extinction in all cases except for iPTF15ul and SN 2011kl. SN 2011kl was associated with GRB 111209A, and the afterglow emission has been subtracted.

References. (1) Vinkó et al. 2015; (2) Greiner et al. 2015; (3) Kann et al. 2019; (4) Arcavi et al. 2016; (5) Hosseinzadeh et al. 2017; (6) Pursiainen et al. 2018; (7) Whitesides et al. 2017; (8) Prentice et al. 2018; (9) Perley et al. 2019a.
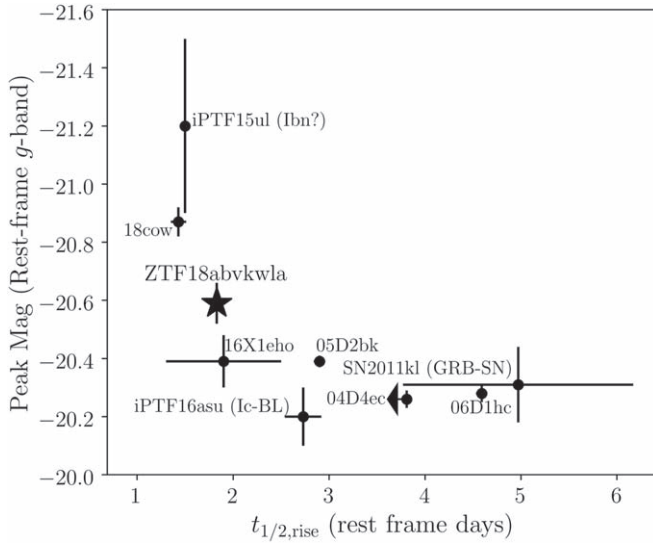

Figure 1. Phase space of luminosity and rise time considered in this paper; see Table 1 for data sources. We do not show the transient Dougie (Vinkó et al. 2015), which had a peak absolute magnitude of -23. Note that the peak mag of iPTF15ul includes a large host-galaxy extinction correction, whereas the other sources have zero host extinction correction. Also note that SN 2011kl was associated with an ultra-long duration GRB 111209A (Kann et al. 2018), and the light-curve properties shown here reflect the afterglow-subtracted light curve (Kann et al. 2019).

2.1.2. Spectroscopy and Host Galaxy Properties

One day after discovery, we obtained a spectrum of ZTF18abvkwla using the Double Beam Spectrograph (DBSP; Oke & Gunn 1982) on the 200 inch Hale telescope at Palomar Observatory. We used the D55 dichroic, a slit width of 1.5 arcseconds, the 600/4000 blue grating, and the 316/7500 red grating. The spectrum was reduced using a PyRAF-based pipeline (Bellm & Sesar 2016). As shown in Figure 5, the spectrum shows a hot blue continuum with no broad features in emission or absorption. Superimposed on the spectrum are a variety of narrow emission lines typical of a star-forming galaxy (Hα, Hβ, O III, S II, O II) at a redshift of $z = 0.2714$ plus the Mg II UV doublet in absorption at consistent redshift.

A blackbody fit to the continuum (after subtracting a host-galaxy continuum model, discussed later in this section) indicates an effective temperature $T \gtrsim 40{,}000$ K, although
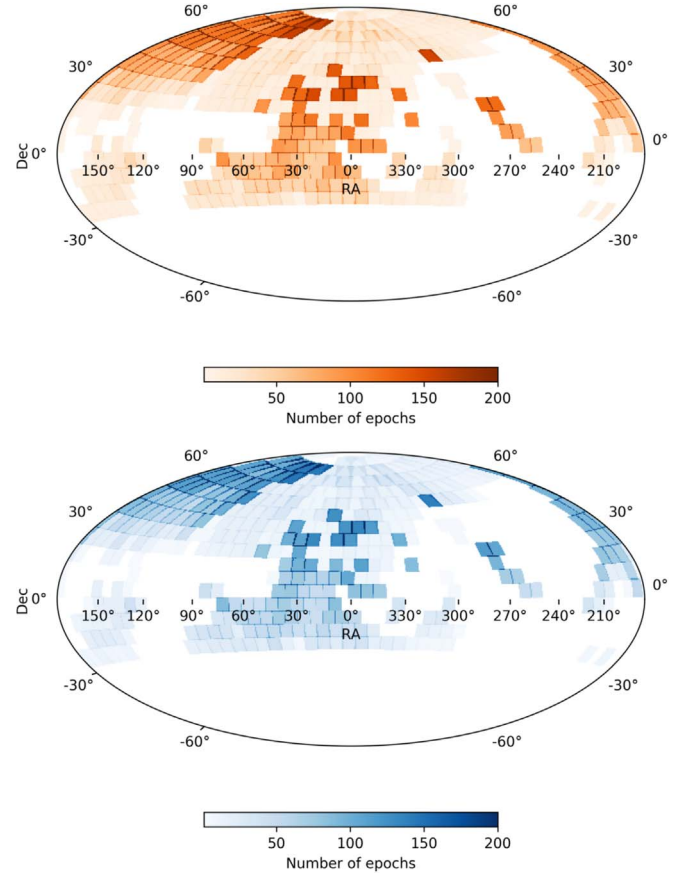
Figure 2. Number of epochs obtained by the ZTF one-day cadence survey from 2018 April 3 to 2019 October 18

we caution that it could be significantly higher, as the bulk of the energy was clearly emitted in the UV (<2750 Å in the rest frame) and we have no firm constraint on the host-galaxy extinction. Together with the peak absolute magnitude of the g-band light curve, we derive a bolometric luminosity of $L_{\rm bol} > \nu L_\nu \sim 10^{44}$ erg s^{-1}. Assuming $T = 40{,}000$ K, the photospheric radius is $R > 2 \times 10^{14}$ cm. Because the peak is two days after first light, assuming $R(t = t_0) = 0$ gives $V > 0.04c$.
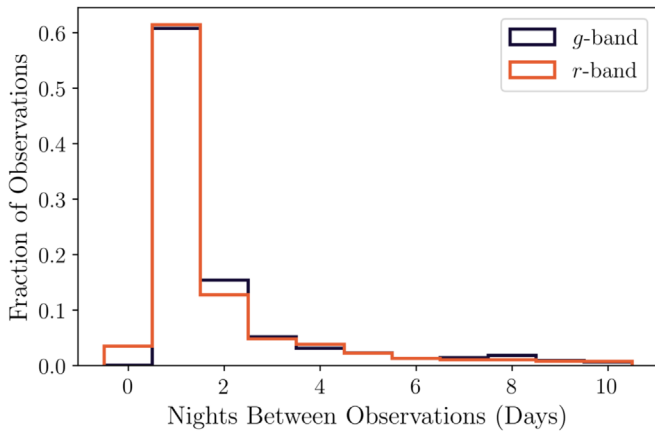
Figure 3. Histogram of times between successive observations of a field in the same filter for the ZTF one-day cadence survey. Intervals greater than 10 days are not shown.

On 2019 January 4 (+115 days), we obtained a spectrum of the host galaxy of ZTF18abvkwla using the Low Resolution Imaging Spectrometer (Oke et al. 1995; McCarthy et al. 1998) on the Keck I 10 m telescope, with the 400/3400 grism in the blue camera and the 400/8500 grating in the red camera. Exposure times were 940 and 900 s for the blue and red cameras, respectively. The spectrum was reduced and extracted using `Lpipe` (Perley 2019). The absolute calibration was established independently for each camera (red versus blue) by calculating synthetic photometry of the output spectra in the blue and red cameras in the g and r bands, respectively, and rescaling to match the g and r photometry from SDSS DR14 (Abolfathi et al. 2018). The SDSS magnitudes (AB, converted to Pogson) are $u = 21.74 \pm 0.20$ mag, $g = 21.20 \pm 0.04$ mag, $r = 20.81 \pm 0.05$ mag, $i = 20.92 \pm 0.09$ mag, and $z = 20.52 \pm 0.20$ mag.

The host-galaxy spectrum (Figure 6) consists of a weak continuum and a series of very strong emission lines. Line fluxes were extracted using a procedure identical to that in Perley et al. (2016). We first fit a model to the spectral energy distribution (SED). We used a custom IDL routine based on the templates of Bruzual & Charlot (2003) to fit the SDSS $ugriz$ photometry, including the contribution of nebular lines. As only SDSS $ugriz$ photometry is available to fit the host-galaxy SED, it is difficult to constrain the nature of the stellar population of the host galaxy in detail, and we were only able to fit the simplest possible model (a continuous star formation history). However, the stellar mass is unambiguously low ($\sim 5 \times 10^8 M_\odot$, comparable to the SMC),

This model was then used to produce a synthetic galaxy continuum spectrum, which was subtracted from the observed one (this correction is significant only for higher-order Balmer lines, which overlay strong galaxy absorption features). Emission line fluxes were then measured by fitting a Gaussian function to each emission line (plus a linear baseline to fit any continuum residuals). Lines that were blended or very nearby were fit in groups, and lines whose ratios are fixed from theory were tied together in fitting. A list of all measured line fluxes is given in Table 3.

The SED fitting and the emission-line analysis produce consistent estimates of $7 M_\odot$ yr^{-1} for the star formation rate, and a very high specific star formation rate of $\sim 10^{-8}$ yr^{-1}. This implies a stellar population dominated by young stars formed in a recent triggered star formation burst episode.

We used the host galaxy spectrum (Figure 6) to calculate standard emission-line diagnostics, including metallicity estimates on a variety of scales using the Monte Carlo code of Bianco et al. (2016). The metallicity measurements are provided in Table 4. The basic properties of the host galaxy are listed in Table 5.

2.2. Radio Observations

We obtained four epochs of observations of ZTF18abvkwla using the Karl G. Jansky Very Large Array (VLA; Perley et al. 2011) under the program VLA/18B-242 (PI: D. Perley), listed in Table 6. The first epoch was at $\Delta t \approx 81$ days at X-band, while the VLA was in C configuration. We used 3C138 as our flux density and bandpass calibrator, and J0204+1514 as our complex gain calibrator. The next three epochs were at $\Delta t \approx 310$ days, $\Delta t \approx 350$ days, and $\Delta t \approx 400$ days, all while the VLA was in A configuration. For these three epochs we continued to use 3C138, but switched to J0238 + 1636 as our complex gain calibrator. For each observation, we ran the standard VLA calibration pipeline available in the Common Astronomy Software Applications (CASA; McMullin et al. 2007). After calibration, we inspected the data manually for further flagging. We imaged the data using the CLEAN algorithm (Högbom 1974) available in CASA, using a cell size that was one-fifth of the synthesized beamwidth. The field size was set to be the smallest magic number (10×2^n) larger than the number of cells needed to cover the primary beam.

In addition, the position of ZTF18abvkwla was serendipitously covered by the VLA Sky Survey (VLASS; Lacy et al. 2020), which has been mapping the entire sky visible to the VLA at low frequencies (2–4 GHz) in three epochs at a cadence of 32 months. The Quicklook images are now available for the first epoch (17,000 deg^{-2}). We searched the existing Quicklook data using code available on Github[18] that locates the appropriate VLASS tile and subtile for a given R.A. and decl. and extracts a cutout 12″ on a side. Given a nondetection, we estimated an upper limit on the flux density by taking the standard deviation of the pixel values in this cutout, after performing initial 3σ clipping (removing pixels with a value greater than $3\times$ the standard deviation). The VLASS observation of ZTF18abvkwla is also listed in Table 6.

We obtained one epoch of observations with the upgraded Giant Metrewave Radio Telescope (GMRT; Swarup 1991; Gupta et al. 2017) under a proposal for Director's Discretionary Time (Proposal # ddtC086; PI: A. Ho). For our GMRT observations, we used 3C147 and 3C48 as our flux density and bandpass calibrators and 0238+166 for our phase calibrator. We calibrated the GMRT data manually using commands in CASA, with six rounds of phase-only self-calibration and two rounds of amplitude and phase self-calibration.

The radio light curve from the VLA is shown in Figure 7. At the time of our first observation, the 10 GHz (rest-frame 12 GHz) luminosity was 10^{30} erg s^{-1} Hz^{-1}, and the in-band spectral index was $\alpha = 0.16 \pm 0.05$, where $F_\nu \propto \nu^\alpha$. At late times ($\Delta t > 300$ days), the decline is very steep: at 6 GHz, we find $F_\nu \propto t^{-6.8 \pm 0.9}$, and at 10 GHz, we find $F_\nu \propto t^{-3.2 \pm 1.4}$.

To estimate the contribution to the radio emission from the host galaxy, we use the relation in Greiner et al. (2016),

---

[18] https://github.com/annayqho/Query_VLASS
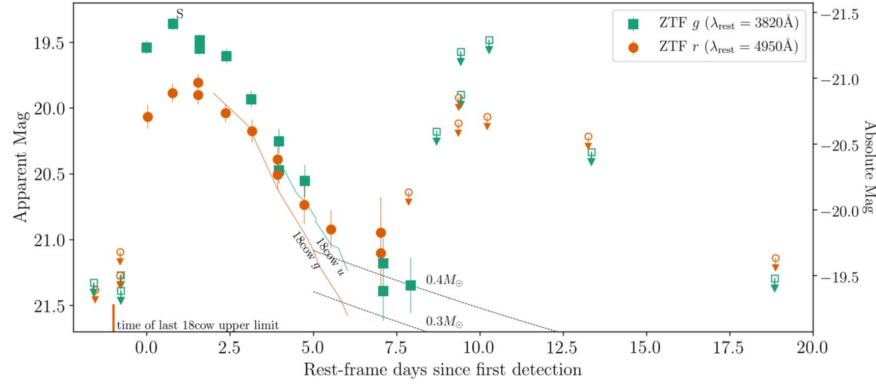
Figure 4. Light curve of ZTF18abvkwla in P48 g (filled green squares) and r (filled orange circles), with a comparison to AT2018cow at similar rest wavelengths, both corrected for Galactic extinction. The "S" at the top of the inset indicates the epoch of our DBSP spectrum. Dashed lines show ^{56}Ni-powered light curves for two different nickel masses.

Table 2
Optical Photometry for ZTF18abvkwla from Forced Photometry on P48 Images (Yao et al. 2019)

Date (MJD)	Δt	Filter	AB Mag
58372.39	−1.02	r	<21.39
58372.42	−0.99	g	<21.56
58373.41	0.00	g	19.71 ± 0.05
58373.45	0.04	r	20.18 ± 0.09
58374.39	0.98	r	20.00 ± 0.07
58374.41	1.00	g	19.53 ± 0.05
58375.37	1.96	r	19.92 ± 0.07
58375.37	1.96	r	20.02 ± 0.07
58375.43	2.03	g	19.65 ± 0.04
58375.43	2.03	g	19.72 ± 0.05
58376.42	3.01	r	20.15 ± 0.07
58376.44	3.04	g	19.77 ± 0.05
58377.39	3.98	g	20.10 ± 0.07
58377.43	4.02	r	20.29 ± 0.09
58378.40	4.99	r	20.50 ± 0.10
58378.40	4.99	r	20.62 ± 0.12
58378.45	5.04	g	20.64 ± 0.10
58378.45	5.05	g	20.42 ± 0.09
58379.42	6.02	r	20.85 ± 0.15
58379.44	6.04	g	20.72 ± 0.12
58380.43	7.03	r	21.04 ± 0.15
58382.34	8.93	r	21.06 ± 0.27
58382.34	8.93	r	21.22 ± 0.28
58382.43	9.03	g	21.35 ± 0.19
58382.43	9.03	g	21.56 ± 0.23
58383.48	10.07	g	21.51 ± 0.21

Note. Values have not been corrected for Galactic extinction. Phase Δt is defined from t_0, the last nondetection.

adapted from Murphy et al. (2011):

$$\left(\frac{\mathrm{SFR}_{\mathrm{Radio}}}{M_\odot \, \mathrm{yr}^{-1}}\right) = 0.059 \left(\frac{F_\nu}{\mu \, \mathrm{Jy}}\right)(1+z)^{-(\alpha+1)}$$
$$\times \left(\frac{D_L}{\mathrm{Gpc}}\right)^2 \left(\frac{\nu}{\mathrm{GHz}}\right)^{-\alpha}. \qquad (1)$$

In the final epoch of our radio observations, assuming $\alpha = -0.75$ (Condon 1992) where $F_\nu \propto \nu^\alpha$, the 10 GHz flux density of 0.031 ± 0.003 mJy predicts a SFR of $20 \, M_\odot \, \mathrm{yr}^{-1}$. Therefore, we conclude that during the final observation, the

radio emission is still dominated by the transient, but the host may contribute a nontrivial fraction of the flux.

3. Comparison with Extragalactic Explosions

3.1. Optical Light Curve and Spectrum

As shown in Section 1, the fast rise time and high peak luminosity of ZTF18abvkwla are shared by only a handful of transients in the literature. In this section, we compare the optical properties of ZTF18abvkwla to the transients in Table 1. We exclude Dougie because it resides in an old stellar population with no signs of enhanced star formation (Vinkó et al. 2015); the dominance of absorption features and much lower star formation rate were confirmed by additional LRIS spectroscopy (Arcavi et al. 2016).

To compare light curves, we selected the light curve in a filter closest to rest-frame g (the same filters used in constructing Figure 1). Following Whitesides et al. (2017), we calculated absolute magnitudes using

$$M = m_{\mathrm{obs}} - 5 \log_{10}\left(\frac{D_L}{10 \, \mathrm{pc}}\right) + 2.5 \log_{10}(1+z). \qquad (2)$$

We cannot perform a true K-correction because most objects lack sufficient spectroscopic coverage. These equations will introduce systematic errors on the order of 0.1 mag.

In Figure 8, we show the rest-frame g-band light curve of ZTF18abvkwla compared to the light curves of transients in Table 1. The fast rise time of ZTF18abvkwla is most similar to that of iPTF15ul, AT2018cow, and perhaps iPTF16asu: it is faster than SN 2011kl and the SNLS transients. ZTF18abvkwla fades much more quickly than iPTF16asu (which spectroscopically evolved into a Ic-BL SN), and in this sense is more similar to iPTF15ul and AT2018cow. In terms of peak luminosity, ZTF18abvkwla is close to iPTF15ul, AT2018cow, DES16X1eho, and iPTF16asu, and brighter than SN 2011kl and the SNLS transients. However, we caution that the high peak luminosity of iPTF15ul results from a large host-galaxy extinction inferred in Hosseinzadeh et al. (2017), without which the peak magnitude would be −19.6 mag.

Next, we consider color evolution. ZTF18abvkwla showed tentative evidence for reddening over time, from $g-r = -0.47 \pm 0.09$ mag at peak to $g-r = -0.03 \pm 0.21$ mag in the final epoch a week later; however, this is only a 2σ change. AT2018cow, iPTF15ul, and DES16X1eho remained
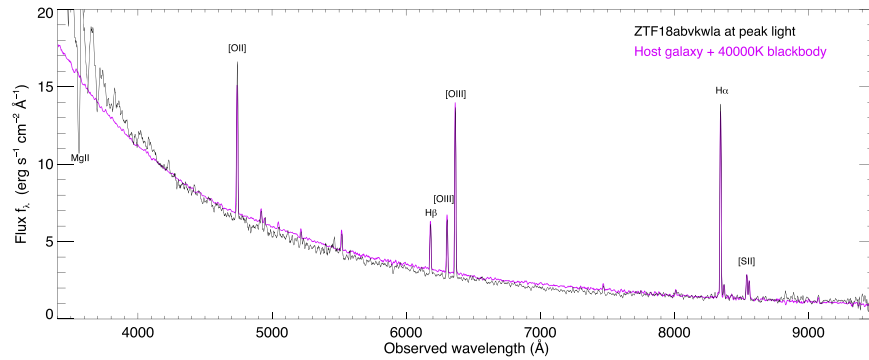
Figure 5. Spectrum of ZTF18abvkwla at the peak of the *g*-band optical light curve (black), which was one day after the first detection. Source is extremely hot and blue, with no spectral features except those associated with the host galaxy. Overplotted in pink is a rescaled late-time spectrum of the host galaxy with a 40,000 K blackbody added.

(The data used to create this figure are available.)

very blue throughout the evolution of their optical light curves, whereas iPTF16asu reddened significantly as the SN became the dominant component.

Finally, we consider the spectral evolution of the transients in Table 1. Peak-light spectra were not obtained for DES16X1eho (Pursiainen et al. 2018) or the SNLS transients (Arcavi et al. 2016). The peak-light spectra of iPTF16asu, AT2018cow, and SN 2011kl were featureless (Greiner et al. 2015; Whitesides et al. 2017; Perley et al. 2019a), and iPTF15ul[19] had a weak emission feature attributed to C III (Hosseinzadeh et al. 2017). After peak, iPTF16asu developed features of a Ic-BL SN (Whitesides et al. 2017), and AT2018cow had a complex spectral evolution, with a broad feature ($v > 0.1c$) that appeared and disappeared over several days following peak light and a variety of emission lines that appeared one week later (Perley et al. 2019a). Unfortunately, we do not have any spectra of ZTF18abvkwla after peak.

3.2. Radio Light Curve

In the previous section (Section 3.1), we compared the optical properties of ZTF18abvkwla to the transients in Table 1: the light-curve shape, the color evolution, and the spectrum. In this section, we compare the radio properties of ZTF18abvkwla to the same set of transients.

Of the transients in Table 1, only AT2018cow and GRB 111209A/SN 2011kl had detected radio counterparts.[20] Prompt radio follow-up observations were also obtained for iPTF15ul[21] and iPTF16asu, but neither was detected. To our knowledge, Dougie, the SNLS transients, and DES16X1eho did not have deliberate radio follow-up observations; we searched the VLASS archive and found that all except SNLS04D4ec were observed but none were detected. In Figure 9, we show the radio measurements of the Table 1 transients compared to stellar explosions and tidal disruption

events. For completeness, we also searched the positions of all of the transients in the two largest collections of unclassified fast-rising luminous optical transients reported to date: PS1 (Drout et al. 2014) and the Dark Energy Survey (Pursiainen et al. 2018). None were detected, and the limits are listed in Table 7.

As shown in Figure 9, ZTF18abvkwla is most similar in luminosity to long-duration GRB afterglows (Berger et al. 2003; Perley et al. 2014). The SED is also similar: in Section 2.2, we found that the SED of ZTF18abvkwla peaked near 10 GHz at $\Delta t = 81$ days, while the SED of GRB 030329 ($z = 0.1685$) peaked at 5 GHz (Berger et al. 2003) at 67 days post-explosion, and the SED of GRB 130427A ($z = 0.340$) peaked at 10 GHz (Perley et al. 2014) at a similar epoch post-explosion.

3.3. A Starburst Host Galaxy

In Sections 3.1 and 3.2, we compared the optical and radio properties of ZTF18abvkwla, respectively, to other transients in the literature. Here, we put its host galaxy properties into context.

Galaxies with very high specific star formation rates (e.g., sSFR $\gtrsim 10^{-8}$ yr^{-1}, our operational definition of a "starburst") contribute a small fraction of star formation in the low-redshift universe (Lee et al. 2009), so the appearance of ZTF18abvkwla in such a galaxy (sSFR $\sim 1.4 \times 10^{-8}$ yr^{-1}) is noteworthy. However, their contribution to low-metallicity star formation is more significant, as they are typically low-mass and therefore low-metallicity (Tremonti et al. 2004). They are also promising candidates to experience a top-heavy IMF (Dabringhausen et al. 2009) and potential sites of enhanced binary or dynamical stellar interactions (van den Heuvel & Portegies Zwart 2013). Each of these mechanisms has been appealed to in attempts to interpret the relatively high abundance of exotic transients of other types found in these systems, including superluminous SNe (SLSNe; Lunnan et al. 2014; Leloudas et al. 2015; Perley et al. 2016; Schulze et al. 2018), broad-lined Ic SNe (Modjaz et al. 2019), GRBs (Fruchter et al. 2006; Krühler et al. 2015; Schulze et al. 2015; Vergani et al. 2015), and at least some fast radio bursts (Katz 2016; Tendulkar et al. 2017).

Based on our measurements in Section 2.1.2, we conclude the following about the host of ZTF18abvkwla:

The host is not an AGN—We confirm the lack of any evidence for an optical AGN based on the very weak [N II]

---

[19] iPTF15ul was classified as Type Ibn in Hosseinzadeh et al. (2017), but the lack of distinct He I at peak make this classification uncertain).

[20] In the case of GRB 111209A/SN 2011kl, the radio emission was likely from the GRB afterglow itself (Kann et al. 2018).

[21] Observations of iPTF15ul were obtained within five days of the optical discovery, two observer-frame days after peak optical light, at 6 GHz and 22 GHz with the VLA, at 15 GHz with the Arcminute Microkelvin Imager (Zwart et al. 2008), and at 95 GHz with the Combined Array for Research in Millimeter-wave Astronomy (Bock et al. 2006). There was no detection at any frequency, with an rms of 0.235 mJy with CARMA and an rms of 0.03 mJy with AMI.
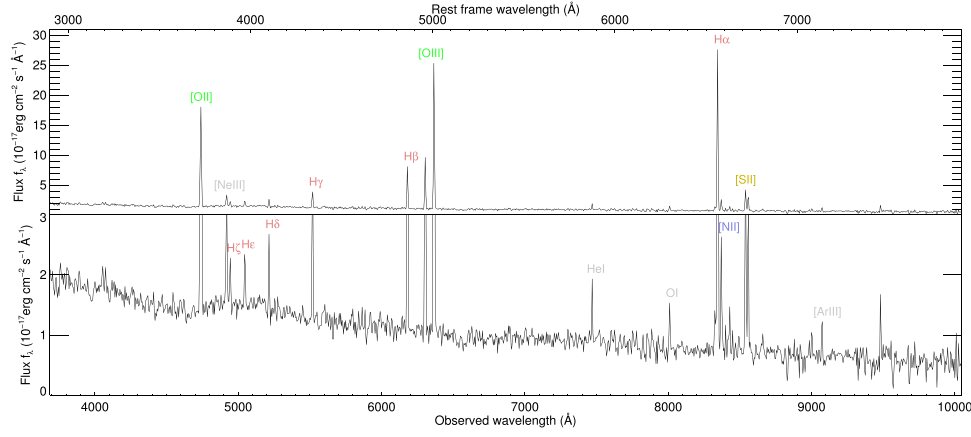
Figure 6. Spectrum of the host galaxy of ZTF18abvkwla. Scale on the bottom half has been zoomed in to show the galaxy continuum and weak emission lines. Feature at 9500 Å is a sky-subtraction residual.

(The data used to create this figure are available.)

Table 3
Host Emission Line Fluxes and Equivalent Widths

Species	Wavelength (Å)	Flux (erg cm^{-2} s^{-1})	Eq. Width (Å)
Hα	6562.82	214.74 ± 2.71	205.9 ± 7.0
Hβ	4861.33	57.57 ± 1.07	41.3 ± 1.1
Hγ	4340.47	26.98 ± 1.03	17.6 ± 0.8
Hδ	4101.74	13.92 ± 0.91	7.2 ± 0.5
Hϵ	3970.08	11.44 ± 0.86	5.9 ± 0.4
Hζ	3889.06	9.72 ± 0.88	5.0 ± 0.5
[O II]	3727	159.44 ± 1.72	89.0 ± 2.4
[Ne III]	3868.76	16.00 ± 0.94	8.3 ± 0.5
[O III]	4363.21	<3.31	<2.1
[O III]	4958.91	66.35 ± 1.37	47.6 ± 1.4
[O III]	5006.84	196.88 ± 1.60	141.3 ± 3.1
He I	5875.62	6.76 ± 0.72	5.7 ± 0.6
[N II]	6548.06	4.90 ± 0.69	4.7 ± 0.7
[N II]	6583.57	13.91 ± 0.82	13.3 ± 0.9
[S II]	6716.44	27.86 ± 0.95	29.3 ± 1.2
[S II]	6730.82	21.81 ± 0.71	22.9 ± 0.9
O I	6300.30	6.76 ± 0.71	7.2 ± 0.8
[Ar III]	7135.79	5.49 ± 0.53	6.8 ± 0.7

Table 4
Host Galaxy Properties (Metallicities, Mainly) from PyMCZ

SFR[a]	6.47 ± 1.3
$E(B-V)$	$0.220^{+0.023}_{-0.022}$
logR23	$0.903^{+0.012}_{-0.012}$
D02	$8.253^{+0.130}_{-0.128}$
Z94	$8.450^{+0.016}_{-0.010}$
M91	$8.219^{+0.026}_{-0.026}$
PP04_N2Ha	$8.200^{+0.010}_{-0.010}$
PP04_O3N2	$8.187^{+0.008}_{-0.009}$
P10_ONS	$8.708^{+0.024}_{-0.024}$
P10_ON	$8.172^{+0.046}_{-0.047}$
M08_N2Ha	$8.361^{+0.020}_{-0.021}$
M08_O3O2	$8.521^{+0.011}_{-0.011}$
M13_O3N2	$8.174^{+0.009}_{-0.009}$
M13_N2	$8.194^{+0.041}_{-0.042}$
KD02_N2O2	$7.567^{+0.722}_{-0.074}$
KK04_N2Ha	$8.381^{+0.028}_{-0.029}$
KK04_R23	$8.390^{+0.021}_{-0.021}$
KD02comb	$8.304^{+0.024}_{-0.024}$

Note.
[a] SFR is not from PyMCZ, but rather is calculated directly from the corrected Balmer-line fluxes based on the relation of Kennicutt et al. (1994).

Table 5
Properties of the Host Galaxy of ZTF18abvkwla

|		
Stellar mass	M	$5.1^{+3.4}_{-2.0} \times 10^8\, M_\odot$
Star formation rate	SFR	$6.8^{+3.7}_{-4.6}\, M_\odot\, \mathrm{yr}^{-1}$
Maximum age	age	$7.5^{+30}_{-4.5} \times 10^7$ yr
Extinction	Av	$0.72^{+0.17}_{-0.54}$ mag
	χ^2/dof	1.6/2
Metallicity	12+log[O/H]	8.5

Notes. Stellar mass, star formation rate, maximum age, and extinction are from a fit to the galaxy SED; the χ^2 refers to that fit. Metallicity [O/H] was measured using the host galaxy spectrum and is provided on the Z94 scale. This value corresponds to 0.6× solar. SFR listed here is derived from the photometry, while the SFR in Table 4 was derived from the spectrum. Thus, there is no expectation of identical values or errors.

emission. The host falls squarely into the star-forming locus of the BPT diagram (Figure 10(a)).

The host metallicity is typical for its mass—The host is relatively metal-poor. The precise number is, of course, scale-dependent, but using the Z94 scale, we calculate [O/H] of 8.45, or about 0.6 × Solar. While this is a lower metallicity than the majority of star formation in the local universe, it is not an outlier, and is unexceptional for low-mass galaxies in particular (Figure 10(b)).

The star formation intensity is similar to extreme SLSN and GRB hosts—The most striking nature of the host galaxy is its very high specific star formation rate, which is evident in Figures 10(c) and (d).

The host of AT 2018cow was also a dwarf galaxy, although it was more massive than that of ZTF18abvkwla and not starbursting, with a mass and star formation rate of $1.4 \times 10^9\, M_\odot$ and $0.22\, M_\odot\, \mathrm{yr}^{-1}$, respectively (Perley et al. 2019a). The host galaxy of DES16X1eho had a stellar mass $\log(M/M_\odot) = 9.96^{+0.14}_{-0.51}$ and a specific SFR of

Table 6
Radio Observations of ZTF18abvkwla with the VLA and the GMRT

Δt (days)	Facility	Obs. Date (UT)	Config.	ν (GHz)	Flux Density (mJy)
81	VLA	2018 Dec 1	C	10	0.364 ± 0.006
188	VLA[a]	2019 Mar 19	B	3	<0.134
310	VLA	2019 Jul 19	BnA	10	0.061 ± 0.003
343	VLA	2019 Aug 21	A	6	0.089 ± 0.003
346	VLA	2019 Aug 24	A	3	0.068 ± 0.004
351	VLA	2019 Aug 29	A	1.5	0.146 ± 0.013
352	VLA	2019 Aug 30	A	10	0.045 ± 0.003
364	GMRT	2019 Sep 11	⋯	0.6	<0.105
396	VLA	2019 Oct 13	A	10	0.031 ± 0.003
397	VLA	2019 Oct 14	A	6	0.033 ± 0.003

Notes. Upper limit is reported as 3× the image rms.
[a] From VLASS.
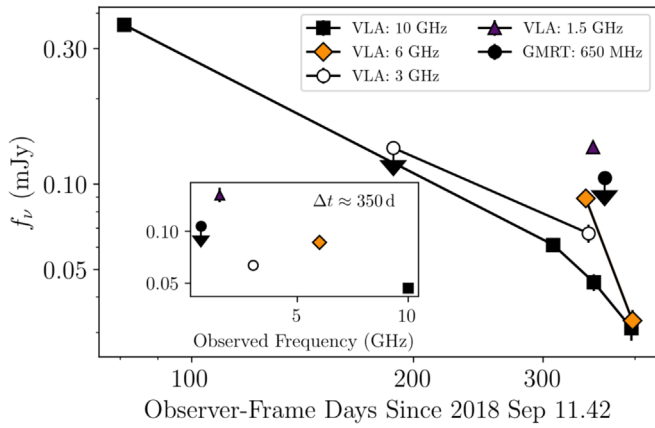
Figure 7. Radio light curve of ZTF18abvkwla with the spectral energy distribution at $\Delta t \approx 350$ days (rest-frame $\Delta t \approx 275$ days) shown inset. Upper limit at 3 GHz comes from a serendipitous observation by VLASS.
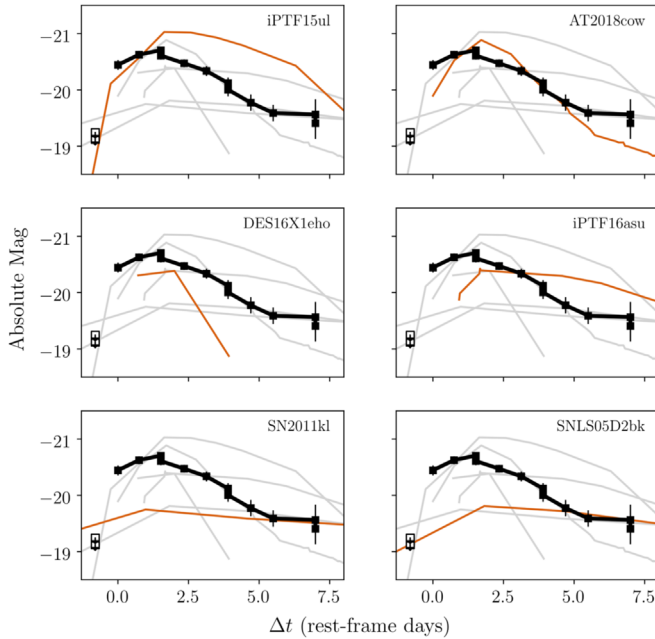
Figure 8. Rest-frame g-band (observer-frame r-band) light curve of ZTF18abvkwla (black line), compared to light curves of other transients in the literature in as close to the same rest-frame filter as possible. Each panel shows one transient highlighted in orange for comparison, with the rest shown in gray in the background.
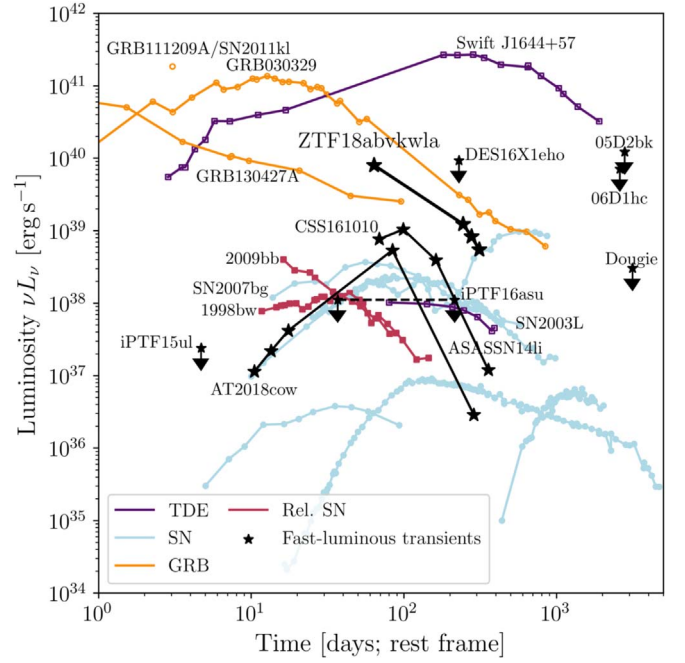
Figure 9. The 10 GHz radio light curve of ZTF18abvkwla compared to low-frequency (1–10 GHz) light curves of different classes of energetic explosions: tidal disruption events (purple; Zauderer et al. 2011; Berger et al. 2012; Zauderer et al. 2013; Alexander et al. 2016; Eftekhari et al. 2018), supernovae exploding in dense CSM (blue lines, $\gtrsim 10^{37}$ erg s^{-1}; Soderberg et al. 2005, 2006; Salas et al. 2013), relativistic Ic-BL supernovae (red lines; Kulkarni et al. 1998; Soderberg et al. 2010), AT2018cow (black line, small stars), long-duration gamma-ray bursts (orange lines; Berger et al. 2003; Hancock et al. 2012; Perley et al. 2014; van der Horst et al. 2014), and "ordinary" supernovae ($\lesssim 10^{37}$ erg s^{-1}; Weiler et al. 1986, 2007; Krauss et al. 2012; Horesh et al. 2013). CSS161010 light curve was taken from Coppejans et al. (2020). AT2018cow light curve is at 9 GHz, with data taken from Ho et al. (2019b), Margutti et al. (2019), and Bietenholz et al. (2020).

$\log(\mathrm{sSFR/M_\odot\ yr^{-1}}) = -9.25$ (Pursiainen et al. 2018). The host galaxy of iPTF16asu had a stellar mass $M = 4.6^{+2.0}_{-2.3} \times 10^8\ M_\odot$ and an Hα SFR of 0.7 $M_\odot$ yr^{-1}, corresponding to a sSFR of 1.4 Gyr^{-1} (Whitesides et al. 2017). Finally, the host galaxies of the SNLS transients harbored relatively evolved stellar populations, and were noted to be markedly different from starburst galaxies (Arcavi et al. 2016).

4. Interpretation

Even with the small number of events in the Table 1 menagerie, the diversity of optical and radio properties (Sections 3.1 and 3.2) suggests that there are several progenitor systems involved. In this section, we model the optical and radio light curves of ZTF18abvkwla and discuss the implications for the progenitor.

4.1. Modeling the Optical Light Curve

Shock interaction with extended low-mass material is an efficient mechanism for producing a fast-peaking luminous optical light curve. Shock breakout occurs when the photon diffusion time drops below the shock crossing time ($\tau < c/v_s$, where τ is the optical depth and v_s is the shock velocity). For normal stellar progenitors, this emission is primarily at X-ray and UV wavelengths and lasts for seconds to a fraction of an hour. In the wake of this shockwave, the outer stellar material is

Table 7
Radio Limits for Rapidly Evolving Transients in Drout et al. (2014) and
Pursiainen et al. (2018)

ID	z	R.A. (hh:mm:ss)	Decl. (dd:mm:ss)	Δt (days)	Limit (μJy)
PS1-10ah	0.074	10:48:15.784	+57:24:19.48	2836	102
PS1-11qr	0.324	09:56:41.767	+01:53:38.25	2467	130
PS1-12bb	0.101	09:57:23.866	+03:11:04.47	2174	149
PS1-12bv	0.405	12:25:34.602	+46:41:26.97	2642	129
PS1-12brf	0.275	22:16:06.892	−00:58:09.81	1892	124
PS1-11bbq	0.646	08:42:34.733	+42:55:49.61	2731	159
PS1-13duy	0.27	22:21:47.929	−00:14:34.94	1505	127
PS1-13dwm	0.245	22:20:12.081	+00:56:22.35	1422	155
PS1-10iu	⋯	16:11:34.886	+55:08:47.91	2689	103
PS1-13aea	⋯	12:18:14.320	+47:20:12.60	2199	88
PS1-13 bit	⋯	16:12:00.765	+54:16:08.16	1618	104
PS1-13cgt	⋯	16:18:56.245	+54:19:33.71	1552	123
DES15S1fli	0.45	02:52:45.15	−00:53:10.21	826	150
DES13X3gms	0.65	02:23:12.27	−04:29:38.35	1520	139
DES15S1fll	0.23	02:51:09.36	−00:11:48.71	826	139
DES14S2anq	0.05	02:45:06.67	−00:44:42.77	1199	118
DES14X3pkl	0.3	02:28:50.64	−04:48:26.44	1100	105
DES15C3lpq	0.61	03:30:50.89	−28:36:47.08	849	145
DES16S1dxu	0.14	02:50:43.53	−00:42:33.29	385	154
DES15C3mgq	0.23	03:31:04.56	−28:12:31.74	835	99
DES16X1eho	0.76	02:21:22.87	−04:31:32.64	365	152
DES16X3cxn	0.58	02:27:19.32	−04:57:04.27	393	128
DES15C3lzm	0.33	03:28:41.86	−28:13:54.96	839	106
DES13C3bcok	0.35	03:32:06.47	−28:37:29.70	1513	98
DES15C3nat	0.84	03:31:32.44	−28:43:25.06	810	108
DES15C3opk	0.57	03:26:38.76	−28:20:50.12	777	125
DES15C3opp	0.44	03:26:57.53	−28:06:53.61	781	112
DES13X3npb	0.5	02:26:34.11	−04:08:01.96	1411	122
DES16C3axz	0.23	03:31:14.15	−28:40:00.25	523	100
DES16C3gin	0.35	03:31:03.06	−28:17:30.98	391	107
DES14X1bnh	0.83	02:14:59.79	−04:47:33.32	1172	145
DES16X3ega	0.26	02:28:23.71	−04:46:36.18	357	111
DES15C3mfu	⋯	03:28:36.08	−28:44:20.00	835	187
DES13C3abtt	⋯	03:30:28.91	−28:09:42.12	1513	107
DES15C3pbi	⋯	03:28:56.68	−28:00:07.98	772	182
DES15X3atd	⋯	02:23:21.64	−04:17:28.95	830	146
DES13C3nxi	⋯	03:27:51.22	−28:21:26.21	1559	75
DES13C3smn	⋯	03:27:53.08	−28:05:00.93	1564	124
DES13X3aakf	⋯	02:22:50.84	−04:41:57.01	1441	108
DES13X3afjd	⋯	02:28:00.31	−04:34:59.39	1411	123
DES13X3kgm	⋯	02:26:00.92	−04:51:59.29	1508	103
DES16S2fqu	⋯	02:47:05.94	−00:20:50.40	356	139
DES16X1ddm	⋯	02:15:18.88	−04:21:52.07	386	111
DES16X3ddi	⋯	02:21:45.39	−04:41:08.95	393	127
DES16X3erw	⋯	02:24:49.31	−04:30:51.45	357	117

Note. Here, Δt is the number of days between the discovery (Drout et al. 2014) or the time of peak (Pursiainen et al. 2018) and the epoch of the VLASS observation of that field.

heated to high temperatures, and as it cools, it radiates on the timescale of a day ("cooling envelope" emission). See Waxman & Katz (2017) for a review.

Prior to core collapse, massive stars can undergo mass loss via steady winds or eruptive episodes (Smith 2014). As a result, a star can be surrounded by dense, recently expelled material at the time of explosion. If this material is optically thick, it increases the effective radius of the star and prolongs the light curve from shock breakout. If the light curve of ZTF18abvkwla arises from shock breakout in a shell, we can estimate the radius of this extended material (CSM) assuming a rise to peak

bolometric luminosity $t_{\rm rise} < 2$ days, a peak luminosity $L_{\rm bol} > 10^{44}$ erg s^{-1}, and a typical SN shock velocity of 10^4 km s^{-1}. The rise timescale is

$$t_{\rm BO} \sim \frac{R_{\rm CSM}}{v_s}$$

$$= (1.3 \text{ days})\left(\frac{R_{\rm CSM}}{10^{15} \text{ cm}}\right)\left(\frac{v_s}{10^4 \text{ km s}^{-1}}\right)^{-1}. \quad (3)$$

For ZTF18abvkwla, we find $R_{\rm CSM} < 1.5 \times 10^{15}$ cm.

We can also estimate the mass in the shell, assuming that the shock deposits half its kinetic energy $(1/2)\rho v_s^2$ and that this deposited energy is $E_{\rm BO} \sim 4\pi R^2 dR e_s$, where the energy density reflects the amount of thermal energy in the layer. The luminosity scales as

$$L_{\rm BO} \sim \frac{E_{\rm BO}}{t_{\rm cross}} \sim \frac{v_s^3}{4}\frac{dM}{dR} = (2.2 \times 10^{45} \text{ erg s}^{-1})$$

$$\times \left(\frac{v_s}{10^4 \text{ km s}^{-1}}\right)^3\left(\frac{dM}{M_\odot}\right)\left(\frac{dR}{10^{15} \text{ cm}}\right)^{-1}. \quad (4)$$

Assuming $dR \sim R$, we find $M_{\rm CSM} < 0.07\, M_\odot$. In this framework, the differences in the light curves of different objects correspond to differences in the shell mass, shell radius, and shock velocity. The luminosity is most sensitive to the velocity, so it is possible that the transients in Table 1 are distinguished by fast velocities, which would naturally explain the inclusion of a Ic-BL SN. For a fixed shock velocity, a fast rise time corresponds to a small shell radius, which in turn requires a large shell mass to produce a high luminosity.

Another possibility is that the light curve is powered not by shock breakout in a shell, but rather by post-shock envelope-cooling emission. For example, this was the model invoked for iPTF16asu (Whitesides et al. 2017), which led to an inferred shell mass of 0.45 $M_\odot$ and a shell radius of 1.7×10^{12} cm. The light curve of ZTF18abvkwla has a similar rise time but a higher peak luminosity than that of iPTF16asu, and the effective temperature at peak is significantly higher. According to the one-zone analytic formalism in Nakar & Piro (2014) and Piro (2015), a higher peak temperature for a fixed rise time and a fixed opacity arises from a larger shell radius. A larger shell radius can also explain the higher bolometric luminosity, although that could also arise from a larger explosion energy or faster ejecta velocity.

Another mechanism suggested to explain the optical light curve of AT2018cow was reprocessing by dense outer ejecta (Margutti et al. 2019). In this picture, a central source (such as an accretion disk or magnetar) emits high-energy (i.e., X-ray) emission, which is reprocessed by surrounding material to produce lower-energy (i.e., optical) radiation. Reprocessing is also invoked to explain tidal disruption events, in which case the surrounding material is unbound stellar debris (Strubbe & Quataert 2009). Indeed, several properties of ZTF18abvkwla and AT2018cow are similar to TDEs in the literature, such as the photospheric radius of 10^{14}–10^{15} cm, the effective temperature of 10^4 K, and high radio luminosities For reviews of TDE observations, see Gezari (2012) and Komossa (2015).

Regardless of the power source at peak, we can use the optical light curve to put an upper limit on the mass of ^{56}Ni that could have been synthesized in the explosion. Using Equation (16) in Kasen (2017), the luminosity from the radioactive decay
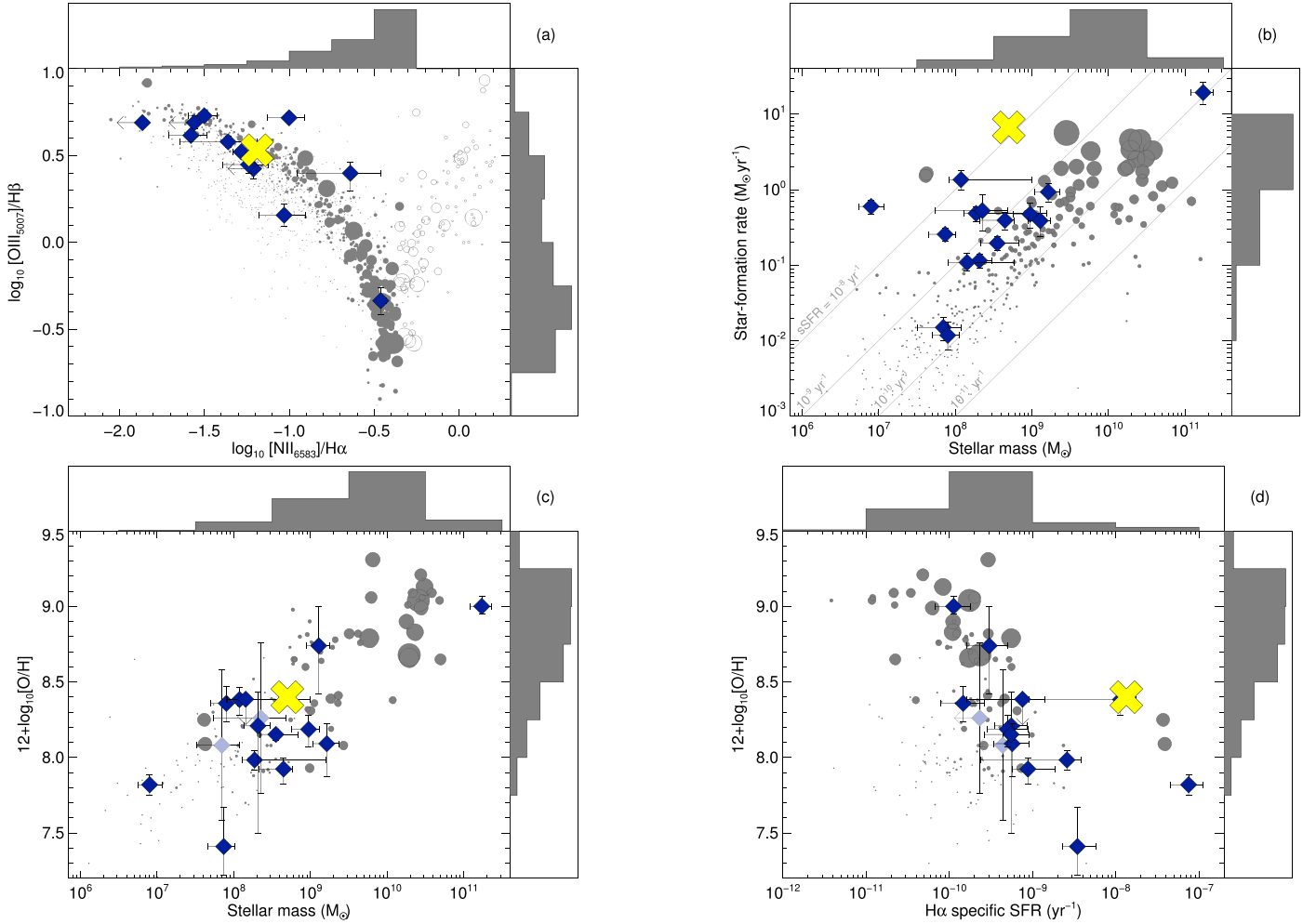
Figure 10. Comparison of the host galaxy of ZTF18abvkwla to <11 Mpc comparison galaxies (gray) and to the host galaxies of nearby hydrogen-poor SLSNe (diamonds), as in Perley et al. (2016). Light diamonds indicate mass–metallicity estimated metallicities. Comparison galaxies are weighted by their SFR; histograms show the SFR-weighted binned totals on each axis. ZTF18abvkwla is indicated by a yellow cross. From top left: (a) BPT diagram; (b) mass–star formation rate relation; (c) mass–metallicity relation; (d) specific star formation-rate–metallicity relation. Host is a starbursting galaxy with no evidence of AGN activity. While it is metal-poor, it is not particularly so given its mass.

of ^{56}Ni is

$$L(t) = 2 \times 10^{43} \left(\frac{M_{\rm Ni}}{M_{\odot}} \right)$$
$$\times \, [3.9 e^{-t/\tau_{\rm Ni}} + 0.678(e^{-t/\tau_{\rm Co}} - e^{-t/\tau_{\rm Ni}})] \; {\rm erg \; s^{-1}}, \quad (5)$$

where $\tau_{\rm Ni} = 8.8$ days and $\tau_{\rm Co} = 113.6$ days. Using the final g-band measurement ($g = 21.51 \pm 0.21$) at $\Delta t = 10$ days ($\Delta t = 8$ days rest-frame) $L \approx \lambda F_{\lambda} \approx 1.4 \times 10^{43}$ erg s^{-1}, so the amount of ^{56}Ni that could power the light curve at this epoch is $M_{\rm Ni} \lesssim 0.36 \, M_{\odot}$ (Figure 4). From a compilation of CC SNe, Lyman et al. (2016) found nickel masses of $0.11 \pm 0.04 \, M_{\odot}$ for Type IIb SNe, $0.17 \pm 0.16 \, M_{\odot}$ for Type Ib SNe, $0.22 \pm 0.16 \, M_{\odot}$ for Type Ic SNe, and $0.32 \pm 0.15 \, M_{\odot}$ for Type Ic-BL SNe. Therefore, we cannot rule out an underlying nickel-powered light curve for ZTF18abvkwla.

4.2. Modeling the Radio Light Curve

The high luminosity and fast variability timescale of the 10 GHz light curve implies a high brightness temperature $T_B \approx 10^{11}$ K, so we conclude that the emission is synchrotron

radiation. In the first epoch, the 10 GHz observation is declining and has an in-band (8–12 GHz) spectral index of $\alpha = 0.16 \pm 0.05$ where $F_{\nu} \propto \nu^{\alpha}$. This is much shallower than the optically thick ($\alpha = 2.5$) or the optically thin ($\alpha = -0.7$) regimes of a synchrotron self-absorption (SSA) spectrum, which suggests that the peak of the SED is near 10 GHz (observer-frame) at this epoch. In what follows, we assume that the SSA spectrum has a rest-frame peak frequency $\nu_p \lesssim 8$ GHz (the bottom of the band) and a rest-frame peak flux density $F_p \gtrsim 0.364$ mJy.

When the SSA peak is known, the outer shock radius R_p and magnetic field strength B_p can be derived assuming that energy is equally partitioned into magnetic fields and relativistic electrons (Scott & Readhead 1977; Readhead 1994). We use equations (11) and (12) from Chevalier (1998) to find R_p and B_p for radio SNe. Assuming an optically thin spectral index of ν^{-1} and a filling factor $f = 0.5$, we find $R_p \gtrsim 8.0 \times 10^{16}$ cm and $B_p \lesssim 0.51$ G. Thus, the mean velocity until $t_{\rm obs} = 81$ days is $\Gamma \beta c = R_p(1 + z)/t_{\rm obs} = 0.38c$. Using Equations (12), (16), and (23) from Ho et al. (2019b), and assuming $\epsilon_e = \epsilon_B = 1/3$, we find that the shock has swept up energy $U = 3.4 \times 10^{49}$ erg into an ambient medium of density $n_e = 190$ cm^{-3}, corresponding to a mass-loss rate of $\dot{M} = 5.8 \times 10^{-4} \, M_{\odot}$ yr^{-1},
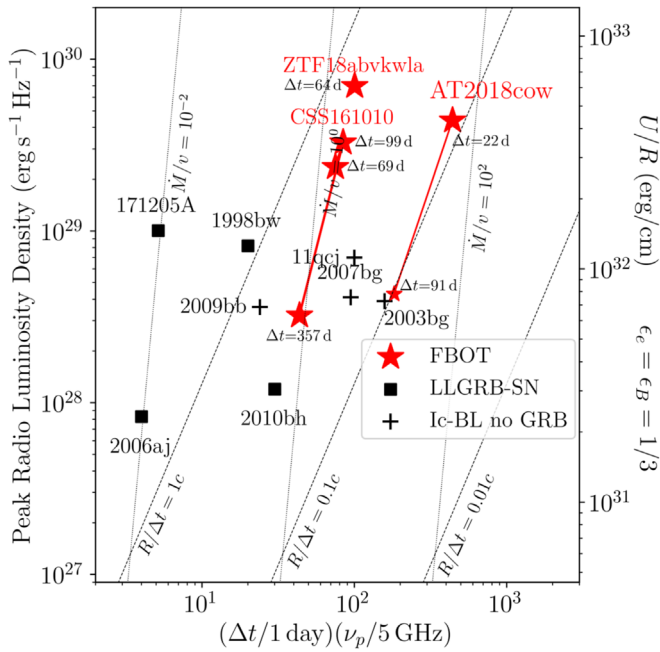
Figure 11. Approximate luminosity and frequency of the SSA peak of ZTF18abvkwla at $\Delta t = 81$ days (observer-frame), compared to other energetic explosions in the literature, including AT2018cow (Ho et al. 2019b; Margutti et al. 2019) and CSS161010 (Coppejans et al. 2020). Lines of constant mass-loss rate are shown in units of $10^{-4}\,M_\odot\,\mathrm{yr}^{-1}$, scaled to a wind velocity of $1000\,\mathrm{km\,s^{-1}}$. Corresponding energy of the explosion (assuming equipartition) is shown on the right-hand side.

assuming a wind velocity $v_w = 1000\,\mathrm{km\,s^{-1}}$. In Figure 11, we show these quantities compared to those of other energetic explosions. The peak radio luminosity density is directly proportional to U/R, the energy swept up by the shock divided by the shock radius (right-hand side of Figure 11). Therefore, the fact that ZTF18abvkwla, AT2018cow, and CSS161010 are distinguished by high radio luminosities is primarily a consequence of a large explosion energy.

4.3. Progenitor Systems and a Search for an Associated Gamma-Ray Burst

The mechanisms outlined in Section 4.1—a shock driven through a shell, reprocessing of a high-energy compact source by optically thick material—could arise in a variety of different progenitor systems. An additional clue for ZTF18abvkwla is the host galaxy, which experienced a very recent burst of star formation activity. In that sense, a massive-star origin seems most natural.

AT2018cow was suggested to have two distinct components: a shock driven through dense equatorial material (producing the optical emission), and a faster polar outflow (producing the radio emission; Margutti et al. 2019). As shown by early millimeter observations (Ho et al. 2019b), later radio observations (Margutti et al. 2019), and Very Long Baseline Interferometry (Bietenholz et al. 2020; Mohan et al. 2020), the fast outflow was subrelativistic with a near-constant velocity of $v = 0.1c$. In ZTF18abvkwla, the radio-emitting ejecta is faster: $>0.38c$ at the same epochs when the outflow velocity of AT2018cow was $0.1c$. As shown in Figure 11, the higher luminosity at late times arises from this faster velocity; the explosion energy of the two events appears to have been similar.

Because the late-time radio light curve is similar of that of GRBs, we searched for potential GRB counterparts to ZTF18abvkwla in the period between the last optical nondetection (MJD 58372.4206; 2018 September 11 10:05:39.84) and the first optical detection (MJD 58373.4075; 2018 September 12 09:46:48.00). There were two bursts detected by the interplanetary network (IPN; Hurley et al. 2010, 2016) during this interval: one by the Gamma-ray Burst Monitor (GBM) on board the Fermi spacecraft (Gruber et al. 2014; von Kienlin et al. 2014; Narayana Bhat et al. 2016), and one by the Konus-Wind experiment on board the Wind spacecraft (Aptekar et al. 1995). The positions of both bursts are inconsistent with that of ZTF18abvkwla.

Due to the lack of detected GRB, we can set a limit on the fluence and corresponding isotropic equivalent energy of a prompt burst associated with ZTF18abvkwla. The IPN has essentially a 100% duty cycle across the sky, and it detects GRBs with $E_p > 20$ keV down to $6 \times 10^{-7}\,\mathrm{erg\,cm^{-2}}$ at 50% efficiency (Hurley et al. 2010, 2016). At t_0, the estimated 20–1500 keV limiting peak flux at the position of ZTF18abvkwla was $2 \times 10^{-7}\,\mathrm{erg\,cm^{-2}\,s^{-1}}$ for a Band model that has E_{pk} in the 50–500 keV range. At the distance of ZTF18abvkwla, this corresponds to a limit on the isotropic peak luminosity of $L_{iso} < 5 \times 10^{49}\,\mathrm{erg\,s^{-1}}$. Therefore, we strongly disfavor an on-axis classical GRB (which is unsurprising given the lack of observed optical afterglow emission).

Among GRBs, two events have shown evidence for a luminous optical blackbody component at early times: GRB 060218 ($z = 0.033$; Ferrero et al. 2006; Mirabal et al. 2006; Pian et al. 2006; Soderberg et al. 2006; Sollerman et al. 2006) and GRB 101225A ($z = 0.847$; Thöne et al. 2011; Levan et al. 2014). GRB 060218 was a very long-duration ($T_{90} \approx 2100$ s) low-luminosity ($L_{iso} = 2.6 \times 10^{46}\,\mathrm{erg\,s^{-1}}$) GRB associated with the Ic-BL SN 2006aj (Cano et al. 2017). A GRB with these properties cannot be ruled out by our limits. GRB 101225A also had a very long duration ($T_{90} > 2000$ s), as well as a candidate SN counterpart.

As in the case of AT2018cow, we cannot rule out a TDE origin. In that case, the similarity to the light curve of AT2018cow would suggest a similar kind of system, i.e., an intermediate-mass black hole ($M \sim 10^4\,M_\odot$; Perley et al. 2019a) with a white dwarf (Kuin et al. 2019) or a solar-type (Perley et al. 2019a) stellar companion. In the case of AT2018cow, the main argument against a TDE hypothesis was the large ambient density ($10^5\,\mathrm{cm^{-3}}$) from millimeter (Ho et al. 2019b) and radio (Margutti et al. 2019) observations. For ZTF18abvkwla, assuming that the flat spectral index indicates a 10 GHz peak at 81 days, we find a much lower density ($10^2\,\mathrm{cm^{-3}}$). Among TDEs, the radio light curve of ZTF18abvkwla is most similar to that of the TDE candidate IGR J12580+0134 (Irwin et al. 2015), which had a nearly identical νL_ν (and fade rate) one year post-discovery. The radio emission from IGR J12580 + 0134 has been attributed to an off-axis relativistic jet (Irwin et al. 2015; Lei et al. 2016) but interpretation is complicated by the coincidence of the source with a known AGN.

5. Rate Estimate

An important clue to the progenitor of sources like ZTF18abvkwla is the cosmological rate. Furthermore, three fast luminous transients—SN 2011kl (associated with

Table 8
Filtering Criteria for Sources Similar to ZTF18abvkwla in the ZTF 1DC Survey

Criteria	# Sources Remaining
Real,[a] bright,[b] pos. sub.,[c] not star[d]	758,528
Short duration[e] and peak resolved[f]	659

Notes.
[a] `drb > 0.99`.
[b] `magpsf < 20`.
[c] `isdiffpos="t"` or "1."
[d] Not(`sgscore1 > 0.76` and `distpsnr1 < 1`).
[e] Duration between 1 and 100 days.
[f] Peak has preceding or subsequent detection/nondetection in a ± 5 days window that is at least 0.75 mag fainter.

GRB 111209A), AT2018cow, and ZTF18abvkwla–have detected luminous radio emission, although the radio emission from SN 2011kl likely arose from the GRB afterglow. Clearly, being able to recognize additional members of this phase-space in optical surveys would be valuable for radio follow-up observations. In this section, we conduct an archival search of 18 months of the 1DC survey (2018 April 3–2019 October 18 UT) to estimate the rate of transients in the phase space of Figure 1 and delineate false positives.

First, we select field-nights in the survey for which the 1-night coverage was approximately maintained. Specifically, we require:

1. at least one observation the night before ($0.5 < dt < 1.5$ days);
2. at least one observation two nights before ($2.5 < dt < 1.5$ days);
3. at least three observations in the next five nights ($dt < 5.5$ days).

We find 8064 fields satisfying these criteria. Of these, 6854 fields (85%) have limiting magnitude >19.75 mag and 4596 fields (57%) have limiting magnitude >20.5 mag. The dominant effect is lunation, with some night-to-night variations due to weather.

For each of the 8064 field nights, we search for fast transients. To detect a fast transient, we require that the peak of the light curve be "resolved," i.e., that there are measurements both before and after peak light that are >0.75 mag fainter than the peak magnitude. We then measure the time from 0.75 mag below peak to peak by linearly interpolating the light curve. If this rise time is <5 days, we include the transient in our sample. More specifically, we filter sources as summarized in Table 8. We scan the remaining 659 sources by eye and remove sources with very noisy light curves or flaring behavior.

In Table 9, we list all 27 sources with rise times faster than 5 days, including ZTF18abvkwla itself. Five sources are spectroscopically classified SNe: two Type II, two Type Ibn, and one Type IIb. Three sources are classified as CVs: two spectroscopically and one by cross-matching with the AAVSO International Variable Star Index VSX (Watson et al. 2017). Two are very likely flare stars based on previous detections in Pan-STARRS individual-epoch images, and a third is a likely flare star based on a GALEX counterpart. Nine sources are likely extragalactic (based on proximity to a host galaxy). We obtained redshifts for some of these galaxies using LRIS on 2020 February 17. Two sources remain without definitive redshift estimates, so we provide a photometric redshift from

LegacySurvey DR8. One source (ZTF18abxxeai) has a very faint host classified as a PSF in LegacySurvey DR8, and the remaining five sources have no clear host counterpart.

Of the sources with a definitive host redshift measurement, ZTF18abvkwla is the only one that is more luminous than $M = -20$ mag. Clearly, the primary interlopers in searches for transients like ZTF18abvkwla are CVs and less luminous SNe. CVs can be ruled out on the basis of repeated flaring, whereas less luminous SNe can only be ruled out if the redshift of the host galaxy is known *a priori*. Aside from ZTF18abvkwla, eight transients in our sample remain as possibly having $M_{g,peak} < -20$, although the lack of an obvious host for six of them suggests that they are likely CVs.

We take eight as an upper limit for the number of transients in ZTF that could fall within the phase space of Figure 1. Of these, three peak brighter than 19 mag, and four have a peak between 19 and 19.75 mag. We now calculate two all-sky rates. First, we assume that the transient peaks at <19 mag, in which case we discard field nights with a limiting magnitude shallower than 19.75 mag. Next, we assume that the transient peaks at <19.75 mag, in which case we discard field nights with a limiting magnitude shallower than 20.5 mag.

Each ZTF field is $47 \deg^2$, but there is latitude-dependent overlap that has to be taken into account when converting this to a rate per square degrees in the sky. For the primary grid, a rough estimate of the fill factor is 87.5%. For the 1DC survey, the footprint is 10% smaller than the number of fields multiplied by 47 square degrees. Taking fill factor and overlap into account, we estimate a typical area per field of $37 \deg^2$. Thus, for transients brighter than 19 mag, we have $2.5 \times 10^5 \deg^2$ days, and for transients brighter than 19.75 mag, we have $1.7 \times 10^5 \deg^2$ days. For transients peaking brighter than 19 mag, we have a limiting all-sky rate

$$3 \times \frac{41253 \deg^2}{2.5 \times 10^5 \deg^2 \text{ days}} \times \frac{365 \text{ days}}{1 \text{ yr}} \approx 180 \text{ yr}^{-1}. \quad (6)$$

For transients peaking brighter than 19.5 mag, we have a limiting all-sky rate

$$4 \times \frac{41253 \deg^2}{1.7 \times 10^5 \deg^2 \text{ days}} \times \frac{365 \text{ days}}{1 \text{ yr}} \approx 350 \text{ yr}^{-1}. \quad (7)$$

Now, we use the limiting magnitude to estimate a volumetric rate. Assuming a transient that peaks at $M = -20$ mag, requiring a peak apparent magnitude brighter than 19 mag restricts our sensitivity to 400 Mpc. Thus, we find a volumetric rate of $7 \times 10^{-7} \text{ yr}^{-1} \text{ Mpc}^{-3}$. Requiring a peak apparent magnitude brighter than 19.75 mag restricts our sensitivity to 560 Mpc, leading to a volumetric rate of $4 \times 10^{-7} \text{ yr}^{-1} \text{ Mpc}^{-3}$. For reference, we provide local rates of core-collapse SNe and GRBs in Table 10. The rate of events like ZTF18abvkwla appears to be at least two orders of magnitude smaller than the CC SN rate, and more similar to the rate of GRBs in the local universe.

6. Prospects for Detecting X-Ray Emission

Clearly, radio observations are an important avenue of follow-up for transients like ZTF18abvkwla. Another valuable avenue is X-ray observations, which were not obtained for ZTF18abvkwla. We can estimate what the predicted X-ray luminosity would be from inverse Compton scattering, using

Table 9
Fast-rising Transients in ZTF Resulting from Our Archival Search of the One-day Cadence Survey

ZTF Name (IAU Name)	Redshift	Peak Mag	t_{rise}	t_{fade}	Type	Notes
18abvkwla	0.2714	−20.59 ± 0.07	1.83 ± 0.05	3.12 ± 0.22	FBOT	This paper
19aavbjfp (SN2019fkl)	0.028	−17.4 ± 0.4	3.2 ± 0.9	21.8 ± 6.1	SN II*	
19abgbdcp (AT2019lbv)	0.0318	−18.36 ± 0.03	2.32 ± 0.03	14.4 ± 0.9	SN II	
18aalrxas	0.0588	−18.43 ± 0.03	1.86 ± 0.02	2.4 ± 0.3	SN IIb	Fremling et al. (2019)
19abuvqgw (AT2019php)	0.087	−18.9 ± 0.1	3.6 ± 0.1	4.5 ± 0.3	SN Ibn	
19aapfmki (SN2019deh)	0.05469	−19.90 ± 0.01	4.38 ± 0.03	7.2 ± 0.4	SN Ibn	
18abskrix	Galactic	17.78 ± 0.02	1.26 ± 0.03	2.5 ± 0.2	CV	Spectroscopic classification
18absrffm (AT2018ftw)	Galactic	16.34 ± 0.01	2.60 ± 0.03	5.00 ± 0.03	CV	Spectroscopic classification
18abyzkeq	Galactic	18.32 ± 0.10	1.37 ± 0.04	0.93 ± 0.06	CV	AAVSO Name: CSS 151114:224934+375554
18ablxawt	Galactic	18.31 ± 0.04	2.4 ± 0.3	5.2 ± 0.9	Likely flare star	Previous detection in PS1 DR2 at $i = 19.4$
19abpwygn	…	16.74 ± 0.01	2.03 ± 0.03	1.73 ± 0.03	Likely flare star	Previous detection in PS1 DR2 at $z = 18.75$
18abyjgaa	…	18.39 ± 0.03	0.82 ± 0.03	2.05 ± 0.08	Likely flare star	GALEX source, possible flaring in PS1 DR2
18aasaiyp	0.104	−19.13 ± 0.05	1.9 ± 0.6	17.1 ± 0.6	Unknown	
18abuvqgo	0.155	−19.93 ± 0.05	4.7 ± 0.2	9.9 ± 0.6	Unknown	
18abydmfv (AT2018hkr)	0.042	−18.66 ± 0.03	3.15 ± 0.04	7.7 ± 2.5	Unknown	
18acepuyx (AT2018kxh)	0.0711	−19.1 ± 0.2	1.4 ± 0.3	10.8 ± 1.2	Unknown	
19aatoboa(AT2019esf)	0.0758	−18.90 ± 0.03	2.41 ± 0.03	4.9 ± 0.3	Unknown	
19abgbbpx (AT2019leo)	0.0625	−18.83 ± 0.03	4.2 ± 0.3	>5	Unknown	
19abiyyhd (AT2019lwj)	0.07	−18.11 ± 0.05	2.5 ± 0.2	4.1 ± 0.3	Unknown	
19aaadfcp	0.08–0.15	19.04 ± 0.04	2.44 ± 0.15	5.86 ± 0.15	Unknown	
19aanvhyc (AT2019coi)	0.056–0.076	18.41 ± 0.04	4.39 ± 0.04	12.1 ± 2.1	Unknown	
18abxxeai		18.55 ± 0.06	1.9 ± 0.1	6.0 ± 0.8	Unknown	"PSF" host in LegacySurvey DR8
18acgnwpo	…	18.90 ± 0.05	0.52 ± 0.03	6.5 ± 0.5	Unknown	No clear host
19aanqqzb	…	16.63 ± 0.04	1.91 ± 0.07	1.2 ± 0.1	Unknown	No clear host
19aaqfdvu	…	19.02 ± 0.06	2.0 ± 0.2	1.6 ± 0.4	Unknown	No clear host
19aaxfqyx	…	18.76 ± 0.03	0.98 ± 0.03	4.68 ± 0.27	Unknown	No clear host
19abfzfbs	…	19.36 ± 0.17	3.7 ± 2.2	13.4 ± 3.2	Unknown	No clear host

Notes. In the redshift column, a range refers to the 68 percentile range on the photometric redshift from LegacySurvey DR8 (we provide a corresponding range of absolute magnitude) and a single value corresponds to a spectroscopic redshift. When the distance is known, the peak mag is an absolute magnitude, and when the distance is not known, the peak mag is an apparent magnitude. These values correspond to the filter as close to rest-frame g-band as possible, and when the distance is not known, they correspond to the observed g-band filter. Magnitudes are corrected for Galactic extinction and timescales are in rest-frame when the redshift is known, and in observer-frame when the redshift is not known.

Table 10
Local ($z = 0$) Rates of Core-collapse Supernovae and GRBs

Class	Rate/Fraction	References
SN II	$4.47 \pm 1.39 \times 10^{-5}$ yr^{-1} Mpc^{-3}	(1)
SN Ibc	$2.58 \pm 0.72 \times 10^{-5}$ yr^{-1} Mpc^{-3}	(1)
Frac. of Ibc SN that are Ic	0.69 ± 0.09	(2), (3)
Frac. of Ic SN that are Ic-BL	0.21 ± 0.05	(2), (3)
LLGRB	$2.3^{+4.9}_{-1.9} \times 10^{-7}$ yr^{-1} Mpc^{-3}	(4)
	$3.3^{+3.5}_{-1.8} \times 10^{-7}$ yr^{-1} Mpc^{-3}	(5)
ℓGRB	$\mathcal{R}_{obs} = 4.2^{+9.0}_{-4.0} \times 10^{-10}$ yr^{-1} Mpc^{-3}	(6)
	$f_b = 0.0019 \pm 0.0003$	(7)
	$f_b = 0.013 \pm 0.004$	(8)

Notes. Approximately 30% of CC SNe arise from a progenitor stripped of its hydrogen envelope. Among these stripped events, there are roughly equal numbers of IIb, Ib, and Ic events. Of the Ic events, ~10% are "broad-lined," with photospheric velocities $\gtrsim$30,000 km s^{-1}. The fraction of Ic-BL SNe with associated GRBs has been estimated to be 1/40 (Graham & Schady 2016), although the rate is highly uncertain. The fraction of Ic-BL SNe with associated LLGRBs also remains uncertain. Note that the rate quoted for LLGRBs does not include a beaming correction.
References. (1) Li et al. 2011; (2) Kelly & Kirshner 2012; (3) Graham & Schady 2016; (4) Soderberg et al. 2006; (5) Liang et al. 2007; (6) Lien et al. 2014; (7) Frail et al. 2001; (8) Guetta et al. 2005.

the optical and radio luminosities:

$$\frac{L_X}{L_{radio}} = \frac{u_{ph}}{u_B}. \qquad (8)$$

Taking $L_{radio} = 10^{40}$ erg s^{-1}, $u_{ph} = 10^{44}$ erg s$^{-1}/(4\pi R^3/3)$ where $R = 10^{14}$ cm, and $u_B = B^2/8\pi$ where $B = 0.6$ G, we find $L_X \approx 10^{43}$ erg s^{-1}. This is even more luminous than the X-ray emission observed accompanying AT2018cow, which had $L_X \approx 10^{42}$ erg s^{-1} (Rivera Sandoval et al. 2018; Ho et al. 2019b; Margutti et al. 2019). To our knowledge, there were no X-ray follow-up observations of DES16X1eho, while observations of iPTF16asu resulted in an X-ray upper limit of 10^{43} erg s^{-1}. Hosseinzadeh et al. (2017) report pre-peak UV measurements from Swift for iPTF15ul, but to our knowledge, X-ray observations have not been reported. We measured an upper limit of 0.005 count s^{-1} in a single epoch from the publicly available Swift data. Assuming $n_H = 1.7 \times 10^{20}$ cm^{-2} and a power-law source model with a photon index $\Gamma = 2$, we obtain an upper limit on the unabsorbed 0.3–10 keV luminosity of 2×10^{42} erg s^{-1}.

7. Summary and Conclusions

ZTF18abvkwla is distinguished by two key characteristics: a fast-evolving optical light curve with a hot ($T > 40,000$ K) and featureless thermal spectrum at peak, and a long-lived, fast-fading radio light curve similar to those of jet-powered long-duration GRBs. The host galaxy underwent a recent star-

forming episode and has a very high specific star formation rate, similar to that of extreme SLSN and GRB hosts. Events like ZTF18abvkwla are rare: from one year of the ZTF 1DC survey, we estimate that the rate is at least 2–3 orders of magnitude smaller than the CC SN rate.

Due to the lack of late-time photometry, we cannot conclude whether the late-time light curve was powered by the same mechanism as the peak or whether another mechanism such as nickel decay became dominant, and we have only tentative evidence for color evolution (cooling) over time. Furthermore, we cannot determine whether this source developed supernova features, nor whether it most closely resembles a Ic-BL like iPTF16asu, a continuum with emission lines like the Ibn iPTF15ul or the SN/TDE candidate AT2018cow, or neither.

Among the fast luminous optical transients in Table 1, only AT2018cow and SN 2011kl had detected radio emission. ZTF18abvkwla thus adds to the very small number of events in the literature established to have fast blue optical light curves, as well as a separate fast ejecta component that produces luminous radio emission. Interestingly, most of the well-studied transients in Table 1 are associated with a candidate engine-powered explosion. AT2018cow had a long-lived central engine that powered a fast ($0.1c$) outflow. The Koala likely had a central engine that powered an even faster ($>0.38c$) outflow, perhaps a relativistic jet. Source iPTF16asu was a Ic-BL SN, and therefore by definition had faster ejecta velocities than ordinary core-collapse supernovae, although there was no evidence for a jet. SN 2011kl had a burst of high-energy emission (GRB 111209A) and an associated luminous afterglow. Given the sensitivity of the luminosity to the shock speed (Equation (7)), perhaps this apparent relationship between engine-driven supernovae and fast luminous optical transients should not be surprising.

At $z = 0.27$, ZTF18abvkwla was much more distant than AT2018cow ($z = 0.0141$), but the lesson from Section 2.2 and Section 5 is that we should not be deterred by cosmological distances in pursuing X-ray and radio follow-up observations. The radio emission from ZTF18abvkwla would be easily detectable by the VLA out to $z = 0.5$ (assuming 5 μJy rms in half an hour of integration time) or even out to $z = 0.8$ (when it would be 30 μJy). Assuming a Swift/XRT sensitivity limit of 4×10^{-14} erg cm^{-2} s^{-1}, the X-ray emission from ZTF18abvkwla may have been on the detection threshold. For a Chandra sensitivity limit an order of magnitude deeper, this may be on the detection threshold at $z = 0.7$. At these larger distances ($z = 0.5$, $z = 0.7$), the optical g-band magnitudes would be 21.1 and 22.3, respectively. This is out of reach for current surveys like ZTF, but standard for LSST. The false positives in such a search are lower-luminosity explosions (Type IIb, II, and Ibn SNe) and CVs. These can be ruled out via knowledge of the host redshift (and therefore intrinsic luminosity), so we stress the need for extensive and reliable galaxy-redshift catalogs.

The code used to produce the results described in this paper was written in Python and is available online in an open source repository.[22]

---

that the summit of Maunakea has always had within the indigenous Hawaiian community. We are most fortunate to have the opportunity to conduct observations from this mountain.

Facilities: Keck:I (LRIS), Hale (DBSP), EVLA, GMRT.

Software: `Astropy` (Astropy Collaboration et al. 2013, 2018), `IPython` (Pérez & Granger 2007), `matplotlib` (Hunter 2007), `numpy` (Oliphant 2006), `scipy` (Virtanen et al. 2019), `extinction` (Barbary 2016), `LPipe` (Perley 2019), `PYRAF-DBSP` (Bellm & Sesar 2016), `IDLAstro`.

Appendix A
Light-curve Measurements

To construct Table 1, we used observed bands as close as possible to rest-frame g: g-band for $z < 0.15$, r-band for $0.15 < z < 0.45$, i-band for $0.45 < z < 0.78$, and z-band for $0.78 < z < 1.0$. We excluded transients with $z > 1.0$. We measured the rise time from, and the fade time to, 0.75 mag below peak by linearly interpolating the single-filter light curve, and measured uncertainties using a Monte Carlo with 1000 realizations of the light curve. Additional notes on each transient are below.

For iPTF15ul ($z = 0.066$; Hosseinzadeh et al. 2017), the uncertainty on the peak magnitude was dominated by the uncertainty from the host-galaxy extinction estimate. For AT2018cow ($z = 0.0141$; Prentice et al. 2018; Perley et al. 2019a), we used the period of three days between the last nondetection and the first detection as an upper limit on the rise time, although we note that interpolation would give 0.4 days, which is much shorter. We also corrected for 0.287 mag of Galactic extinction, which was not applied in Table 3 of Perley et al. (2019a). For a lower limit, we used the o-band detection before peak (dominated by r-band flux at this epoch), corrected for 0.198 mag of Galactic extinction. We assumed $g - r = -0.4$ mag and $g - i = -0.7$ mag.

For SN 2011kl ($z = 0.677$), we used column M_{4556} in Table 2 of Kann et al. (2019). These values are corrected for rest-frame extinction, and the contributions from the GRB afterglow and host galaxy have been subtracted. For SNLS04D4ec ($z = 0.593$), SNLS05D2bk ($z = 0.699$), and SNLS06D1hc ($z = 0.555$), we used the i-band light curve from Arcavi et al. (2016) and corrected for Milky Way extinction.

For Dougie ($z = 0.19$; Vinkó et al. 2015), we added an additional 0.1 mag in quadrature to account for the zero-point uncertainty, and we corrected for 0.031 mag of Milky Way extinction. For iPTF16asu ($z = 0.187$; Whitesides et al. 2017), we could not measure the rise or peak magnitude in rest-frame g because observations in the appropriate filter (r) began only three days after peak. We estimated an upper limit to the peak magnitude by assuming that the $g - r$ color at peak was identical to the $g - r$ color during the first r-band measurement. We used the first r-band measurement as a lower limit. For the time from half-max to max, we used the observed g-band light curve instead. We obtained the i-band light curve of DES16X1eho ($z = 0.76$; Pursiainen et al. 2018) from M. Pursiainen (2020, private communication).

ORCID iDs

Anna Y. Q. Ho ⬣ https://orcid.org/0000-0002-9017-3567
Daniel A. Perley ⬣ https://orcid.org/0000-0001-8472-1996
Poonam Chandra ⬣ https://orcid.org/0000-0002-0844-6563
Eric C. Bellm ⬣ https://orcid.org/0000-0001-8018-5348
Dmitry D. Frederiks ⬣ https://orcid.org/0000-0002-1153-6340
Christoffer Fremling ⬣ https://orcid.org/0000-0002-4223-103X
V. Zach Golkhou ⬣ https://orcid.org/0000-0001-8205-2506
Matthew J. Graham ⬣ https://orcid.org/0000-0002-3168-0139
Mansi M. Kasliwal ⬣ https://orcid.org/0000-0002-5619-4938
Russ R. Laher ⬣ https://orcid.org/0000-0003-2451-5482
Frank J. Masci ⬣ https://orcid.org/0000-0002-8532-9395
A. A. Miller ⬣ https://orcid.org/0000-0001-9515-478X
Ben Rusholme ⬣ https://orcid.org/0000-0001-7648-4142
David L. Shupe ⬣ https://orcid.org/0000-0003-4401-0430
Maayane T. Soumagnac ⬣ https://orcid.org/0000-0001-6753-1488
Dmitry S. Svinkin ⬣ https://orcid.org/0000-0002-2208-2196

References

Abolfathi, B., Aguado, D. S., Aguilar, G., et al. 2018, ApJS, 235, 42
Alexander, K. D., Berger, E., Guillochon, J., Zauderer, B. A., & Williams, P. K. G. 2016, ApJL, 819, L25
Aptekar, R. L., Frederiks, D. D., Goleneckii, S. V., et al. 1995, SSRv, 71, 265
Arcavi, I., Wolf, W. M., Howell, D. A., et al. 2016, ApJ, 819, 35
Astropy Collaboration, Price-Whelan, A. M., Sipőcz, B. M., et al. 2018, AJ, 156, 123
Astropy Collaboration, Robitaille, T. P., Tollerud, E. J., et al. 2013, A&A, 558, A33
Barbary, K. 2016, extinction, v0.3.0, Zenodo, 10.5281/zenodo.804967
Bellm, E. C., Kulkarni, S. R., Barlow, T., et al. 2019a, PASP, 131, 068003
Bellm, E. C., Kulkarni, S. R., Graham, M. J., et al. 2019b, PASP, 131, 018002
Bellm, E. C., & Sesar, B. 2016, pyraf-dbsp: Reduction pipeline for the Palomar Double Beam Spectrograph, Astrophysics Source Code Library, ascl:1602.002
Berger, E., Kulkarni, S. R., Pooley, G., et al. 2003, Natur, 426, 154
Berger, E., Zauderer, A., Pooley, G. G., et al. 2012, ApJ, 748, 36
Bianco, F. B., Modjaz, M., Oh, S. M., et al. 2016, A&C, 16, 54
Bietenholz, M. F., Margutti, R., Coppejans, D., et al. 2020, MNRAS, 491, 4735
Bock, D. C.-J., Bolatto, A. D., Hawkins, D. W., et al. 2006, Proc. SPIE, 6267, 626713
Bruzual, G., & Charlot, S. 2003, MNRAS, 344, 1000
Cano, Z., Wang, S.-Q., Dai, Z.-G., & Wu, X.-F. 2017, AdAst, 2017, 8929054
Cenko, S. B., Kulkarni, S. R., Horesh, A., et al. 2013, ApJ, 769, 130
Chevalier, R. A. 1998, ApJ, 499, 810
Condon, J. J. 1992, ARA&A, 30, 575
Coppejans, D. L., Margutti, R., Terreran, G., et al. 2020, arXiv:2003.10503
Dabringhausen, J., Kroupa, P., & Baumgardt, H. 2009, MNRAS, 394, 1529
Dey, A., Schlegel, D. J., Lang, D., et al. 2019, AJ, 157, 168
Drout, M. R., Chornock, R., Soderberg, A. M., et al. 2014, ApJ, 794, 23
Duev, D. A., Mahabal, A., Masci, F. J., et al. 2019, MNRAS, 489, 3582
Eftekhari, T., Berger, E., Zauderer, B. A., et al. 2018, ApJ, 854, 86
Ferrero, P., Kann, D. A., Zeh, A., et al. 2006, A&A, 457, 857
Fitzpatrick, E. L. 1999, PASP, 111, 63
Fox, O. D., & Smith, N. 2019, MNRAS, 488, 3772
Frail, D. A., Kulkarni, S. R., Sari, R., et al. 2001, ApJL, 562, L55
Fremling, C., Ko, H., Dugas, A., et al. 2019, ApJL, 878, L5
Fruchter, A. S., Levan, A. J., Strolger, L., et al. 2006, Natur, 441, 463
Gezari, S. 2012, in EPJ Web of Conf. 39, Tidal Disruption Events and AGN Outbursts, ed. R. Saxton & S. Komossa (Les Ulis: EDP Sciences), 03001
Graham, J. F., & Schady, P. 2016, ApJ, 823, 154
Graham, M. J., Kulkarni, S. R., Bellm, E. C., et al. 2019, PASP, 131, 078001
Greiner, J., Mazzali, P. A., Kann, D. A., et al. 2015, Natur, 523, 189
Greiner, J., Michałowski, M. J., Klose, S., et al. 2016, A&A, 593, A17
Gruber, D., Goldstein, A., Weller von Ahlefeld, V., et al. 2014, ApJS, 211, 12
Guetta, D., Piran, T., & Waxman, E. 2005, ApJ, 619, 412
Gupta, Y., Ajithkumar, B., Kale, H. S., et al. 2017, CSci, 113, 707
Hancock, P. J., Murphy, T., Gaensler, B., et al. 2012, GCN, 12804, 1
Ho, A. Y. Q., Goldstein, D. A., Schulze, S., et al. 2019a, ApJ, 887, 169
Ho, A. Y. Q., Phinney, E. S., Ravi, V., et al. 2019b, ApJ, 871, 73
Högbom, J. A. 1974, A&AS, 15, 417

Horesh, A., Stockdale, C., Fox, D. B., et al. 2013, MNRAS, 436, 1258
Hosseinzadeh, G., Arcavi, I., Valenti, S., et al. 2017, ApJ, 836, 158
Huang, K., Shimoda, J., Urata, Y., et al. 2019, ApJL, 878, L25
Hunter, J. D. 2007, CSE, 9, 90
Hurley, K., Golenetskii, S., Aptekar, R., et al. 2010, in AIP Conf. Ser. 1279,
    Deciphering the Ancient Universe with Gamma-Ray Bursts (Melville, NY:
    AIP), 330
Hurley, K., Svinkin, D. S., Aptekar, R. L., et al. 2016, ApJL, 829, L12
Irwin, J. A., Henriksen, R. N., Krause, M., et al. 2015, ApJ, 809, 172
Kann, D. A., Klose, S., Zhang, B., et al. 2010, ApJ, 720, 1513
Kann, D. A., Schady, P., Olivares, E. F., et al. 2018, A&A, 617, A122
Kann, D. A., Schady, P., Olivares, E. F., et al. 2019, A&A, 624, A143
Kasen, D. 2017, Handbook of Supernovae (Cham: Springer), 939
Kasliwal, M. M., Cannella, C., Bagdasaryan, A., et al. 2019, PASP, 131,
    038003
Kasliwal, M. M., Kulkarni, S. R., Gal-Yam, A., et al. 2012, ApJ, 755, 161
Katz, J. I. 2016, MPLA, 31, 1630013
Kelly, P. L., & Kirshner, R. P. 2012, ApJ, 759, 107
Kennicutt, R. C., Tamblyn, P. C., & Congdon, C. E. 1994, ApJ, 435, 22
Komossa, S. 2015, JHEAp, 7, 148
Krauss, M. I., Soderberg, A. M., Chomiuk, L., et al. 2012, ApJL, 750, L40
Krühler, T., Malesani, D., Fynbo, J. P. U., et al. 2015, A&A, 581, A125
Kuin, N. P. M., Wu, K., Oates, S., et al. 2019, MNRAS, 487, 2505
Kulkarni, S. R., Frail, D. A., Wieringa, M. H., et al. 1998, Natur, 395, 663
Lacy, M., Baum, S. A., Chandler, C. J., et al. 2020, PASP, 132, 035001
Law, N. M., Kulkarni, S. R., Dekany, R. G., et al. 2009, PASP, 121, 1395
Lee, J. C., Kennicutt, R. C., Funes, S. J. J. G., et al. 2009, ApJ, 692, 1305
Lei, W.-H., Yuan, Q., Zhang, B., et al. 2016, ApJ, 816, 20
Leloudas, G., Schulze, S., Krühler, T., et al. 2015, MNRAS, 449, 917
Levan, A. J., Tanvir, N. R., Starling, R. L. C., et al. 2014, ApJ, 781, 13
Li, W., Chornock, R., Leaman, J., et al. 2011, MNRAS, 412, 1473
Liang, E., Zhang, B., Virgili, F., et al. 2007, ApJ, 662, 1111
Lien, A., Sakamoto, T., Gehrels, N., et al. 2014, ApJ, 783, 24
Lunnan, R., Chornock, R., Berger, E., et al. 2014, ApJ, 787, 138
Lyman, J. D., Bersier, D., James, P. A., et al. 2016, MNRAS, 457, 328
Lyutikov, M., & Toonen, S. 2019, MNRAS, 487, 5618
Mahabal, A., Rebbapragada, U., Walters, R., et al. 2019, PASP, 131, 038002
Margutti, R., Metzger, B. D., Chornock, R., et al. 2019, ApJ, 872, 18
Masci, F. J., Laher, R. R., Rusholme, B., et al. 2019, PASP, 131, 018003
McCarthy, J. K., Cohen, J. G., Butcher, B., et al. 1998, Proc. SPIE, 3355, 81
McMullin, J. P., Waters, B., Schiebel, D., Young, W., & Golap, K. 2007, adass
    XVI, 376, 127
Miller, A. A., Yao, Y., Bulla, M., et al. 2020, arXiv:2001.00598
Mirabal, N., Halpern, J. P., An, D., et al. 2006, ApJL, 643, L99
Modjaz, M., Bianco, F. B., Siwek, M., et al. 2020, apJ, 892, 153
Mohan, P., An, T., & Yang, J. 2020, ApJL, 888, L24
Murphy, E. J., Condon, J. J., Schinnerer, E., et al. 2011, ApJ, 737, 67
Nakar, E., & Piro, A. L. 2014, ApJ, 788, 193
Narayana Bhat, P., Meegan, C. A., von Kienlin, A., et al. 2016, ApJS, 223, 28
Oke, J. B., Cohen, J. G., Carr, M., et al. 1995, PASP, 107, 375
Oke, J. B., & Gunn, J. E. 1982, PASP, 94, 586
Oke, J. B., & Gunn, J. E. 1983, ApJ, 266, 713
Oliphant, T. E. 2006, A Guide to NumPy (USA: Trelgol Publishing)
Patterson, M. T., Bellm, E. C., Rusholme, B., et al. 2019, PASP, 131, 018001

Pérez, F., & Granger, B. E. 2007, CSE, 9, 21
Perley, D. A. 2019, PASP, 131, 084503
Perley, D. A., Cenko, S. B., Corsi, A., et al. 2014, ApJ, 781, 37
Perley, D. A., Mazzali, P. A., Yan, L., et al. 2019a, MNRAS, 484, 1031
Perley, D. A., Quimby, R. M., Yan, L., et al. 2016, ApJ, 830, 13
Perley, R. A., Chandler, C. J., Butler, B. J., et al. 2011, ApJL, 739, L1
Pian, E., Mazzali, P. A., Masetti, N., et al. 2006, Natur, 442, 1011
Piro, A. L. 2015, ApJL, 808, L51
Planck Collaboration, Ade, P. A. R., Aghanim, N., et al. 2016, A&A, 594, A13
Prentice, S. J., Maguire, K., Smartt, S. J., et al. 2018, ApJL, 865, L3
Pursiainen, M., Childress, M., Smith, M., et al. 2018, MNRAS, 481, 894
Rau, A., Kulkarni, S. R., Law, N. M., et al. 2009, PASP, 121, 1334
Readhead, A. C. S. 1994, ApJ, 426, 51
Rest, A., Garnavich, P. M., Khatami, D., et al. 2018, NatAs, 2, 307
Rivera Sandoval, L. E., Maccarone, T. J., Corsi, A., et al. 2018, MNRAS,
    480, L146
Salas, P., Bauer, F. E., Stockdale, C., & Prieto, J. L. 2013, MNRAS, 428, 1207
Schlafly, E. F., & Finkbeiner, D. P. 2011, ApJ, 737, 103
Schulze, S., Chapman, R., Hjorth, J., et al. 2015, ApJ, 808, 73
Schulze, S., Krühler, T., Leloudas, G., et al. 2018, MNRAS, 473, 1258
Scott, M. A., & Readhead, A. C. S. 1977, MNRAS, 180, 539
Smith, N. 2014, ARA&A, 52, 487
Soderberg, A. M., Chakraborti, S., Pignata, G., et al. 2010, Natur, 463, 513
Soderberg, A. M., Kulkarni, S. R., Berger, E., et al. 2005, ApJ, 621, 908
Soderberg, A. M., Kulkarni, S. R., Nakar, E., et al. 2006, Natur, 442, 1014
Sollerman, J., Jaunsen, A. O., Fynbo, J. P. U., et al. 2006, A&A, 454, 503
Strubbe, L. E., & Quataert, E. 2009, MNRAS, 400, 2070
Swarup, G. 1991, in IAU Coll. 131, Radio interferometry: Theory, techniques,
    and applications (San Francisco, CA: ASP), 376
Tachibana, Y., & Miller, A. A. 2018, PASP, 130, 128001
Tendulkar, S. P., Bassa, C. G., Cordes, J. M., et al. 2017, ApJL, 834, L7
Thöne, C. C., de Ugarte Postigo, A., Fryer, C. L., et al. 2011, Natur, 480, 72
Tremonti, C. A., Heckman, T. M., Kauffmann, G., et al. 2004, ApJ, 613, 898
van den Heuvel, E. P. J., & Portegies Zwart, S. F. 2013, ApJ, 779, 114
van der Horst, A. J., Paragi, Z., de Bruyn, A. G., et al. 2014, MNRAS,
    444, 3151
Vergani, S. D., Salvaterra, R., Japelj, J., et al. 2015, A&A, 581, A102
Vinkó, J., Yuan, F., Quimby, R. M., et al. 2015, ApJ, 798, 12
Virtanen, P., Gommers, R., Oliphant, T. E., et al. 2019, arXiv:1907.10121
von Kienlin, A., Meegan, C. A., Paciesas, W. S., et al. 2014, ApJS, 211, 13
Wang, L. J., Wang, X. F., Cano, Z., et al. 2019, MNRAS, 489, 1110
Watson, C., Henden, A. A., & Price, A. 2017, yCat, 102027, 0
Waxman, E., & Katz, B. 2017, Handbook of Supernovae (Cham:
    Springer), 967
Weiler, K. W., Sramek, R. A., Panagia, N., van der Hulst, J. M., & Salvati, M.
    1986, ApJ, 301, 790
Weiler, K. W., Williams, C. L., Panagia, N., et al. 2007, ApJ, 671, 1959
Whitesides, L., Lunnan, R., Kasliwal, M. M., et al. 2017, ApJ, 851, 107
Yao, Y., Miller, A. A., Kulkarni, S. R., et al. 2019, ApJ, 886, 152
Zackay, B., Ofek, E. O., & Gal-Yam, A. 2016, ApJ, 830, 27
Zauderer, B. A., Berger, E., Margutti, R., et al. 2013, ApJ, 767, 152
Zauderer, B. A., Berger, E., Soderberg, A. M., et al. 2011, Natur, 476, 425
Zwart, J. T. L., Barker, R. W., Biddulph, P., et al. 2008, MNRAS, 391, 1545